



## SELENOK-dependent CD36 palmitoylation regulates microglial functions and A $\beta$ phagocytosis

Pei Ouyang <sup>a,b,1</sup>, Zhiyu Cai <sup>a,1</sup>, Jiaying Peng <sup>a</sup>, Shujing Lin <sup>a</sup>, Xiaochun Chen <sup>a</sup>, Changbin Chen <sup>a</sup>, Ziqi Feng <sup>a</sup>, Lin Wang <sup>c</sup>, Guoli Song <sup>a,b,\*\*</sup>, Zhonghao Zhang <sup>a,b,\*</sup>

<sup>a</sup> Shenzhen Key Laboratory of Marine Bioresources and Ecology, Brain Disease and Big Data Research Institute, College of Life Sciences and Oceanography, Shenzhen University, Shenzhen, China

<sup>b</sup> Shenzhen-Hong Kong Institute of Brain Science-Shenzhen Fundamental Research Institutions, Shenzhen, China

<sup>c</sup> College of Biology and Food Engineering, Anyang Institute of Technology, Anyang, China

### ARTICLE INFO

#### Keywords:

Selenoprotein K  
Amyloid-beta  
Alzheimer's disease  
CD36 palmitoylation  
Microglial phagocytosis

### ABSTRACT

Amyloid-beta (A $\beta$ ) is a key factor in the onset and progression of Alzheimer's disease (AD). Selenium (Se) compounds show promise in AD treatment. Here, we revealed that selenoprotein K (SELENOK), a selenoprotein involved in immune regulation and potentially related to AD pathology, plays a critical role in microglial immune response, migration, and phagocytosis. In vivo and in vitro studies corroborated that SELENOK deficiency inhibits microglial A $\beta$  phagocytosis, exacerbating cognitive deficits in 5xFAD mice, which are reversed by SELENOK overexpression. Mechanistically, SELENOK is involved in CD36 palmitoylation through DHHC6, regulating CD36 localization to microglial plasma membranes and thus impacting A $\beta$  phagocytosis. CD36 palmitoylation was reduced in the brains of patients and mice with AD. Se supplementation promoted SELENOK expression and CD36 palmitoylation, enhancing microglial A $\beta$  phagocytosis and mitigating AD progression. We have identified the regulatory mechanisms from Se-dependent selenoproteins to A $\beta$  pathology, providing novel insights into potential therapeutic strategies involving Se and selenoproteins.

### 1. Introduction

Alzheimer's disease (AD), the most common type of dementia, is neuropathologically characterized by extracellular amyloid-beta (A $\beta$ ) deposition and intracellular neurofibrillary tangles. Despite decades of thorough and extensive research, transformative breakthroughs in the prevention, attenuation, or reversal of AD progression have yet to be realized [1]. The intricate etiology of AD has challenged the precise definition of its pathogenesis, but several studies robustly support the central role of A $\beta$  in triggering the pathological cascade. Therefore, strategies that focus on reducing A $\beta$  production or facilitating its clearance continue to be at the forefront of research and are pivotal in evaluating potential AD therapies [2–5].

Patients with AD and APOE4 allele carriers show reduced levels of selenium (Se), an essential trace element, indicating a significant

correlation between Se levels and AD [6–9]. Therapeutic strategies harnessing Se-centric compounds have yielded promising results in decelerating A $\beta$  and tau pathological progression, restoring synaptic deficits, and ameliorating cognitive impairments in AD models [10–14]. Additionally, our preliminary studies have unveiled the potential mechanistic contributions of Se in countering AD, notably through rectification of autophagic flux, mitochondrial impairments, and oxidative stress [15–18]. Nonetheless, the precise and direct targets of Se in the above effects remain unclear, especially the detailed mechanisms by which Se ameliorates A $\beta$  pathology.

Selenoproteins are universally recognized as the primary biological vectors for Se intracellular activity, orchestrating diverse molecular pathways and physiological processes, including the protection of neurons from oxidative stress and ferroptosis via glutathione peroxidase 4, as well as in the regulation of protein folding and Ca $^{2+}$  homeostasis through endoplasmic reticulum (ER)-resident selenoproteins [19–21].

\* Corresponding author. Shenzhen Key Laboratory of Marine Bioresources and Ecology, Brain Disease and Big Data Research Institute, College of Life Sciences and Oceanography, Shenzhen University, Shenzhen, China.

\*\* Corresponding author. Shenzhen Key Laboratory of Marine Bioresources and Ecology, Brain Disease and Big Data Research Institute, College of Life Sciences and Oceanography, Shenzhen University, Shenzhen, China.

E-mail addresses: [lilys@szu.edu.cn](mailto:lilys@szu.edu.cn) (G. Song), [zzh@szu.edu.cn](mailto:zzh@szu.edu.cn) (Z. Zhang).

<sup>1</sup> These authors contributed equally.

## Abbreviations

A $\beta$	amyloid-beta
AAV	adenovirus
AD	Alzheimer's disease
CM	chloroform-methanol
DAM	disease-associated microglia
DEG	differentially expressed gene
ER	endoplasmic reticulum
FAM-A $\beta$ 42	carboxyfluorescein-A $\beta$ 42
GO	Gene Ontology
GSEA	gene set enrichment analysis

HA	hydroxylamine
HMC3	human microglia cell line clone 3
PFA	paraformaldehyde
SELENOK	selenoprotein K
SELK-KO	selenoprotein K knockout
SELK-OE	selenoprotein K overexpression
SELK-RE	re-expression of selenoprotein K
SeM	selenomethionine
SeNa	sodium selenite
shSELK	selenoprotein K knockdown
WT	wild-type

The dysregulation of these selenoprotein-governed processes has been implicated in the pathogenesis of neurodegenerative diseases. Of the brain-enriched selenoproteins, a significant downregulation of selenoprotein K (SELENOK) is seen in the brains of patients and mice models with AD, which had been confirmed by cognitive deficits in SELENOK knockout mice [22–24]. Nevertheless, few studies have reported on the functional relationship between SELENOK and AD pathology.

Microglia, the intrinsic macrophages in the central nervous system, are pivotal in mounting immune responses in the brain. Early studies on genes associated with AD risk highlighted that nearly all of them are associated with microglial function and metabolism, including *APOE4* and *TREM2* [25,26]. Indeed, microglial activation is implicated in the early stages of AD, contributing to A $\beta$  clearance and degradation [27–29]. Moreover, there is evidence suggesting that A $\beta$ -induced microglial pro-inflammatory activation also exacerbates AD pathology [30–32]. Despite the contradictory outcomes of a plethora of studies on the role of microglia in the onset and progression of AD, there is a consensus that dysregulation of microglial functions is directly related to A $\beta$  pathology [33,34].

SELENOK, localized to the ER membrane and highly expressed in immune cells, is required for the immune response, proliferation, and differentiation of various immune cells [35–37]. Recent in vitro research has shown that SELENOK overexpression markedly augments microglial migration and phagocytosis, indicating a probable impact on central nervous system immunity through microglial modulation [38]. However, these findings remain to be corroborated *in vivo*. The current study aimed to elucidate the regulatory effects of SELENOK on microglial interactions with A $\beta$  aggregates, to understand its implications on neuroimmune homeostasis, and to provide new insights into the role of Se in countering AD.

## 2. Materials and methods

### 2.1. Mice

*Selenok*<sup>−/−</sup> (SELK-KO) mice were generated and bred by Biocytogen (Beijing, China). Wild-type (WT) C57BL/6 J mice used as background controls were purchased from Vital River Laboratories (Beijing, China). Cx3cr1Cre<sup>ERT2</sup> (IMSR\_JAX:021160) and 5xFAD mice (MMRRC\_034848-JAX) were purchased from the Jackson Laboratory (Bar Harbor, ME, USA). AD-SELK-KO mice were generated by crossing 5xFAD mice with SELK-KO mice, and 5xFAD<sup>+/−</sup>/Cx3cr1Cre<sup>ERT2+/−</sup> mice generated by crossing 5xFAD mice with Cx3cr1Cre<sup>ERT2</sup> mice. Mice were housed 5–6 per cage in a pathogen-free mouse facility with ad libitum access to food and water on a 12-h light/dark cycle. The male-to-female ratio was approximately 1:1, unless specified otherwise. Mice from different genotypes were cohoused and did not undergo any procedures prior to their stated use. All procedures were performed in compliance with guidelines approved by the Animal Ethical and Welfare Committee of Shenzhen University (Permit Number: IACUC-202300052).

Adenoviruses (AAVs) were packaged with SELENOK overexpression (SELK-OE) (AAV-MG1.2-SFFV-DIO-mScarlet-P2A-mSelenok [CDS+3'UTR]) and vehicle (AAV-MG1.2-SFFV-DIO-mScarlet) plasmids by Brain Case (Wuhan, China). The plasmids (rAAV/MG1.2 and pAAV-SFFV-DIO-mScarlet) were kindly provided by Dr. Rui Lin (National Institute of Biological Sciences, Beijing, China).

For AAV delivery into the cortex and hippocampus, 10-week-old mice were anesthetized with isoflurane. Each site received  $5 \times 10^9$  vg virus (1  $\mu$ L at  $5 \times 10^{12}$  vg/mL), targeting the right cortex and left hippocampus. The injection coordinates were as follows: cortex – 1.0 mm posterior from the bregma, 2.5 mm lateral, 1.5 mm below the pia mater; hippocampus – 2.0 mm posterior from the bregma, 1.3 mm lateral, 2.2 mm below the pia mater. Following virus administration, tamoxifen (100 mg/kg) (T5648; Sigma-Aldrich, Merck, Germany) was injected intraperitoneally for five consecutive days.

Intraperitoneal injection of Se supplementation in mice: solutions of selenomethionine (SeM; S3875; Sigma-Aldrich, Merck) and sodium selenite (SeNa; 71948; Sigma-Aldrich, Merck) were prepared in saline. Mice were injected with saline, SeM, or SeNa every two days for eight weeks.

### 2.2. Cell culture, treatment, adenovirus, plasmids, and transfection

Human microglia cell line clone 3 (HMC3) cells (Fuheng Biology, Shanghai, China) were maintained in DMEM medium (Gibco, Thermo Fisher Scientific, Waltham, MA, USA) with 10 % FBS (Fuheng Biology). Primary glia cultures were prepared as described previously [32]. Briefly, mixed glial cultures, isolated from postnatal day 1–2 mice, were seeded in poly-L-lysine-coated flasks and cultured in DMEM with 10 % FBS. On day 3, the medium was replaced to include 25 ng/mL GM-CSF and 10 % FBS. Primary microglia were collected after 10–12 days and then every three days by shaking the flask for up to four harvests. Primary astrocytes were isolated after 10 days via overnight shaking to collect adherent cells from the bottom of the culture flask. Approximately  $10^5$  cells were plated into each well of a 6-well plate. Primary neurons were derived from the cortex and hippocampus of E15–17 embryos. The dissociated cells were cultured in neurobasal medium with 2 % B27, 0.5 mM L-glutamine, and 50 U/mL penicillin-streptomycin on poly-L-lysine-coated 6-well plates at a density of  $0.5 \times 10^6$  cells per well. Cultures were used after 12–15 days.

The AAVs employed in this study were engineered by Obio Technology (Shanghai, China). The shRNA construct for SELENOK knockdown (shSELK; GGTGGATGAGGAAGGTAAATG) and the control construct (TTCTCCGAACGTGTCACGT) were under control of the CMV promoter. The SELENOK overexpression virus comprised a CDS (285 bp) coupled with a 3'-UTR (595 bp) (NM\_019979.2). For transfection, cells were plated in 6-well plates and allowed to adhere. The medium was then replaced with 750  $\mu$ L serum-free medium. The virus (virus volume = cell number  $\times$  MOI/virus titer; MOI: 200) was added to each well and incubated for 2 h. Subsequently, 750  $\mu$ L serum-rich medium was added,

and the cells closely observed the next day. Media were refreshed within 24 h. The cells were deemed suitable for downstream experiments 48 h after transfection.

Full-length cDNAs for human CD36 and mutations in its palmitoylation sites were cloned into pcDNA3.1 with C-terminal Flag tags. These plasmids were generated by Obio Technology. Cell transfection commenced at 70–90 % confluence. The plasmid-transfection reagent mixture was prepared as per the manufacturer's instructions, mixed thoroughly, and allowed to stand at room temperature for 20 min. The mixture (500 µL) was gently added to each well, and the medium replaced 4 h later. Cells were evaluated for fluorescence the next day and were ready for further experiments 36 h post-transfection.

### 2.3. Human subjects

Postmortem brain tissues were sourced from the Center for Neurodegenerative Disease Research at the University of Pennsylvania (Philadelphia, PA, USA), with informed consent obtained from all subjects. Demographic details for the patients are available in Table S1. Analyzing the impact of sex and gender identity on the study results was not a focus of this study, and such analysis was not conducted owing to the small sample size.

### 2.4. Isolation of mouse adult microglia and astrocytes from brains

Adult mouse microglia were isolated as previously described [32]. In brief, adult mice were euthanized and perfused with ice-cold PBS. The brains were rinsed, minced, and digested in DMEM/F12 (Gibco, Thermo Fisher Scientific) containing 1 mg/mL papain (P4762; Sigma-Aldrich, Merck), 1.2 U/mL dispase II (D4693; Sigma-Aldrich, Merck), 20 U/mL DNase I (D5025; Sigma-Aldrich, Merck), and 100 U/mL collagenase IV (17104019; Thermo Fisher Scientific) at 37 °C for 30 min. The cell suspension was layered onto a 30 % Percoll (Solarbio, Beijing, China) gradient and centrifuged without rest at 300×g for 30 min at 18 °C. After centrifugation, cells were collected from the bottom layer of the Percoll gradient. After intensive washing, cells were separated using CD11b or ACSA-2 microbeads (Miltenyi Biotec, Germany). The isolated CD11b<sup>+</sup> adult microglia or ACSA-2<sup>+</sup> adult astrocytes were then applied for further analysis.

### 2.5. Immunoblotting

Total protein was extracted from tissues and cells using RIPA buffer, and concentrations measured using a BCA Protein Assay Kit (Beyotime, Nanjing, China). Cellular proteins (approximately 20 µg) were resolved on 10–15 % SDS-PAGE gels and electrotransferred to PVDF membranes (Merck Millipore, Burlington, MA, USA). The membrane was incubated overnight with primary antibodies at 4 °C, followed by a 1-h incubation at 37 °C with HRP-conjugated secondary antibodies (detailed in Table S2). Protein bands were detected using an enhanced chemiluminescence kit (Epizyme, Shanghai, China) and visualized using an automatic chemiluminescence imaging system (Tanon, Shanghai, China). Band intensities were quantified using ImageJ software (National Institutes of Health, Stapleton, NY, USA).

### 2.6. Immunofluorescence and image analyses

After perfusion with 4 % paraformaldehyde (PFA), mouse brains were further fixed in 4 % PFA at 4 °C overnight and subsequently immersed in a 30 % sucrose solution. Brain sections (25 µm thickness) were prepared using a sliding microtome and preserved at –20 °C in a cryoprotectant solution. For immunostaining, both brain sections and

cultured cells were washed thrice with PBS and blocked for 30 min at room temperature in a solution containing 0.5 % Triton X-100 and 10 % normal goat serum. The samples were then incubated overnight at 4 °C with primary antibodies (Table S2) in the blocking buffer. Next, the samples were washed and incubated with secondary antibodies in a blocking buffer for 1 h. After washing, the samples were counterstained with DAPI. Imaging was performed using a ZEISS LSM 880 laser scanning confocal microscope (Carl Zeiss AG, Germany), using z-stack and tile scan features. Acquired images were processed for orthogonal projection or subjected to colocalization channel construction and three-dimensional (3D) reconstruction using Imaris 9.0.1 software (Bitplane, Switzerland).

### 2.7. RNA-seq analysis

Isolated total RNA from adult microglia was used for RNA-seq analysis. The cDNA library construction and sequencing were performed by Jingjie PTM BioLab (Hangzhou, China) using the Illumina platform. High-quality reads were aligned to the mouse reference genome using Hisat2 (v.2.0.5). Each sample was sequenced with a data depth of 10 Gb. Expression levels for each of the genes were quantified using StringTie (v.2.2.0). Differential gene analysis was carried out using the DESeq2 package (v.1.20.0). Differentially expressed genes (DEGs) with ≥2-fold change and p < 0.05 were identified. Gene functional annotation overrepresented by DEGs was performed using the GO (Gene Ontology) database. Gene set enrichment analysis (GSEA) was performed using the ranked list of genes based on the log-fold change obtained from the differential gene analysis.

### 2.8. RNA extraction and quantitative real-time PCR

Total RNA from cells or brain tissues was extracted using RNA-Fast200 (Fastagen Biotech, Shanghai, China) and reverse-transcribed to cDNA using StarScript III All-in-one RT Mix with gDNA Remover (Genstar, Beijing, China), according to the manufacturer's instructions. Relative gene expression was quantified using the 2 × RealStar Fast SYBR qPCR Mix (Genstar) in a CFX Connect Real-Time PCR System (Bio-Rad, Hercules, CA, USA). After normalizing to the reference genes, *Actin* or *GAPDH*, the relative expression levels of the genes were determined. Primer sequences are listed in Table S3.

### 2.9. Flow cytometry

Isolated primary microglia cell suspensions, adult microglia, or HMC3 cells were stained with the indicated antibodies or challenged with fluorescent microspheres. Flow cytometric analysis was performed using CytoFLEX S (Beckman Coulter, Brea, CA, USA) or Calibur (BD Biosciences, Franklin Lakes, NJ, USA). The acquired data was analyzed using FlowJo (version 10.4; BD Biosciences).

### 2.10. Microglial migration in transwell assays

A microglial migration assay was performed in transwell cell culture inserts with an 8-µm pore (Costar, 3422; Corning, NY, USA). Primary microglia and HMC3 cells (10<sup>5</sup>) suspended in serum-free medium were seeded in the upper chamber, with 600 µL serum-free medium added to the lower chamber. One hour post-seeding, the lower chamber medium was replaced with medium containing 10 % serum. The cells were cultured under these conditions for 24 h. Cells on the upper surface of the membrane were removed with a cotton swab, followed by three PBS washes. The cells were then fixed with 4 % PFA for 15 min, washed once with PBS, and stained with 0.1 % crystal violet dye. The total number of

cells on the membrane without scraping was also counted in separate wells. Imaging and quantitative analysis of the results were conducted using Olympus CKX53 (Olympus, Japan) and ImageJ software.

#### 2.11. A $\beta$ 42 oligomer preparation

Synthetic human A $\beta$ 42 (AS-20276; AnaSpec, Fremont, CA, USA) peptides were dissolved in hydroxyfluoroisopropanol and subsequently desiccated using a SpeedVac (Thermo Fisher Scientific). The resultant lyophilized A $\beta$ 42 was reconstituted in dimethyl sulfoxide (D2650; Sigma-Aldrich, Merck) to achieve a 2 mM concentration. This solution was further diluted in DMEM/F12 medium to a final concentration of 200  $\mu$ M. After incubation at 4 °C for 24 h, the A $\beta$ 42 was aliquoted and stored at –80 °C until needed.

Carboxyfluorescein-A $\beta$ 42 (FAM-A $\beta$ 42) (AS-23525; AnaSpec) peptides were dissolved in trifluoroacetic acid, lyophilized using a Speed-Vac, and then redissolved in a DMSO/PBS (1:1) solution to a final concentration of 100  $\mu$ M. The solution was incubated at 37 °C overnight, aliquoted, and stored at –80 °C for later use.

#### 2.12. In vitro phagocytosis assay

Primary microglia, astrocytes, or HMC3 cells were seeded in 6-well plates at a density of  $5 \times 10^5$  cells/well in DMEM supplemented with 10 % FBS. Microspheres (F8823; Thermo Fisher Scientific) or FAM-A $\beta$ 42 oligomers (500 nM) were added to the wells. The cells were co-incubated with microspheres or FAM-A $\beta$ 42 for 3 h at 37 °C in an incubator. Then, cells were washed with PBS and fixed in 1 % PFA for 10 min. Following fixation, the cells were prepared for subsequent flow cytometric analysis.

#### 2.13. In vivo A $\beta$ phagocytosis assay

Mice were intraperitoneally administered methoxy-X04 (4920; Tocris Bioscience, Bristol, UK) at a concentration of 10 mg/kg and dissolved in a 10 % DMSO and 90 % PBS solution (pH 12) for 3 h. Brain single-cell suspensions were prepared as outlined in the “Isolation of mouse adult microglia and astrocytes from brains” section. Cells were then incubated with CD16/CD32 Fc receptor-blocking antibody for 15 min at 4 °C to minimize nonspecific binding. Post-blocking, cells were stained with CD11b-APC (1:100) and CD45-FITC (1:100) in 200  $\mu$ L PBS for 1 h at 4 °C. After a final wash, they were resuspended in 2 % FBS/PBS and subjected to flow cytometry on a CytoFlex S, with data analysis performed via FlowJo. Methoxy-X04-injected WT mice were used as controls to set the threshold for identifying non-phagocytosing cells.

#### 2.14. Intracellular A $\beta$ clearance

Primary microglia were transfected with ADV constructs: vehicle (Control), shSELK, or SELK-OE. Post-transfection, cells were treated with lysosomal enzyme inhibitors (pepstatin A at 10  $\mu$ M, leupeptin at 100  $\mu$ M, and E–64d at 50  $\mu$ M) (HY-P0018, HY-18234, and HY-100229, respectively; MedChemExpress, Monmouth Junction, NJ, USA) or 40  $\mu$ M chloroquine (C6628; Sigma-Aldrich, Merck) for 30 min, followed by incubation with 500 nM A $\beta$ 42 oligomer for 3 h. Post-incubation, cells were trypsinized and washed twice with PBS. Cell lysates were prepared using 5 M guanidine in 50 mM Tris-HCl buffer (pH 8.0) and centrifuged at 12,000  $\times g$  for 25 min at 4 °C. The supernatants were collected for A $\beta$ 42 quantification using ELISA. The degraded A $\beta$ 42 amounts were determined by subtracting the cell-associated A $\beta$  levels without inhibitors from those with inhibitors.

#### 2.15. ELISA

The levels of IL-1 $\beta$  (MLB00C), IL-6 (M6000B), IL-10 (M1000B), IL-4 (404 ML), TNF- $\alpha$  (MTA00B), and A $\beta$ 42 (DAB142) in the brain lysates

were determined using DuoSet ELISA Kits from R&D Systems (Minneapolis, MN, USA), according to the manufacturer’s instructions.

#### 2.16. Morris water maze

The Morris water maze used in this study comprised a 120 cm diameter circular tank filled with tap water maintained at 22 ± 2 °C. Distinct shapes on the tank walls served as spatial cues. During acquisition trials, mice were released from one of four cardinal points (N, S, E, and W) facing the tank wall to find a submerged platform (1–2 cm below water) within 60 s. Mice that failed were guided to the platform and kept there for 10 s. Four trials with 1-h intervals were conducted daily, where the escape latency as a spatial memory indicator was recorded. On the fifth day, a probe test was performed without the platform, measuring time in quadrants, number of platform area crossings, mean speed, and total distance swam.

#### 2.17. Isolation and detection of palmitoylated proteins

Palmitoylated proteins were enriched via the acyl-ABE assay, as previously described [39]. Briefly, 1 mg protein was incubated with 50 mM N-ethylmaleimide overnight at 4 °C. Following three chloroform-methanol (CM) precipitations, the sample was divided into two parts for + hydroxylamine (HA) and -HA treatments. The + HA sample (200  $\mu$ L) was incubated with 800  $\mu$ L Solution A [comprising 700  $\mu$ L of 1 M HA in PBS (pH 7.4), 250  $\mu$ L of 4 mM HPDP-biotin (A8008; APEX BIO, Houston, TX, USA), 20  $\mu$ L of 10 % Triton X-100, 10  $\mu$ L protease inhibitor, and 20  $\mu$ L PBS], whereas the -HA sample (200  $\mu$ L) was treated with 800  $\mu$ L Solution B [containing 250  $\mu$ L of 4 mM HPDP-biotin, 20  $\mu$ L of 10 % Triton X-100, 10  $\mu$ L protease inhibitor, 50  $\mu$ L of 1 M Tris-HCl (pH 7.4), and 670  $\mu$ L PBS], both at 25 °C for 1.5 h. Following another round of CM precipitation, the sample was dissolved in 50  $\mu$ L TB buffer and combined with 0.9 mL LB buffer and 20  $\mu$ L streptavidin-agarose (20353; Thermo Fisher Scientific) at 25 °C for 1.5 h. The precipitates were eluted in 50  $\mu$ L LB containing 1 %  $\beta$ -mercaptoethanol for immunoblot analysis.

#### 2.18. Surface biotinylation

Surface biotinylation was carried out as previously described [40]. Cells ( $5 \times 10^5$ ) in 6-well plates were washed with ice-cold PBS and incubated with freshly prepared sulfo-NHS-SS-biotin (400  $\mu$ L, 0.5 mg/mL) (A8005; APEX BIO) for 30 min on ice. Free sulfo-NHS-SS-biotin was removed by washing the cells thrice with ice-cold quenching buffer (PBS containing 50 mM glycine, pH 7.4). Cells were then lysed in 100  $\mu$ L IP buffer (PBS containing 1 % Triton X-100). The supernatant (20  $\mu$ L) was saved as input, and the remaining 80  $\mu$ L incubated with 10  $\mu$ L streptavidin-agarose and rotated at 4 °C for 2 h. The beads were washed five times with PBS containing 1 % Triton X-100 and eluted in 60  $\mu$ L SDS loading buffer at 65 °C for 10 min.

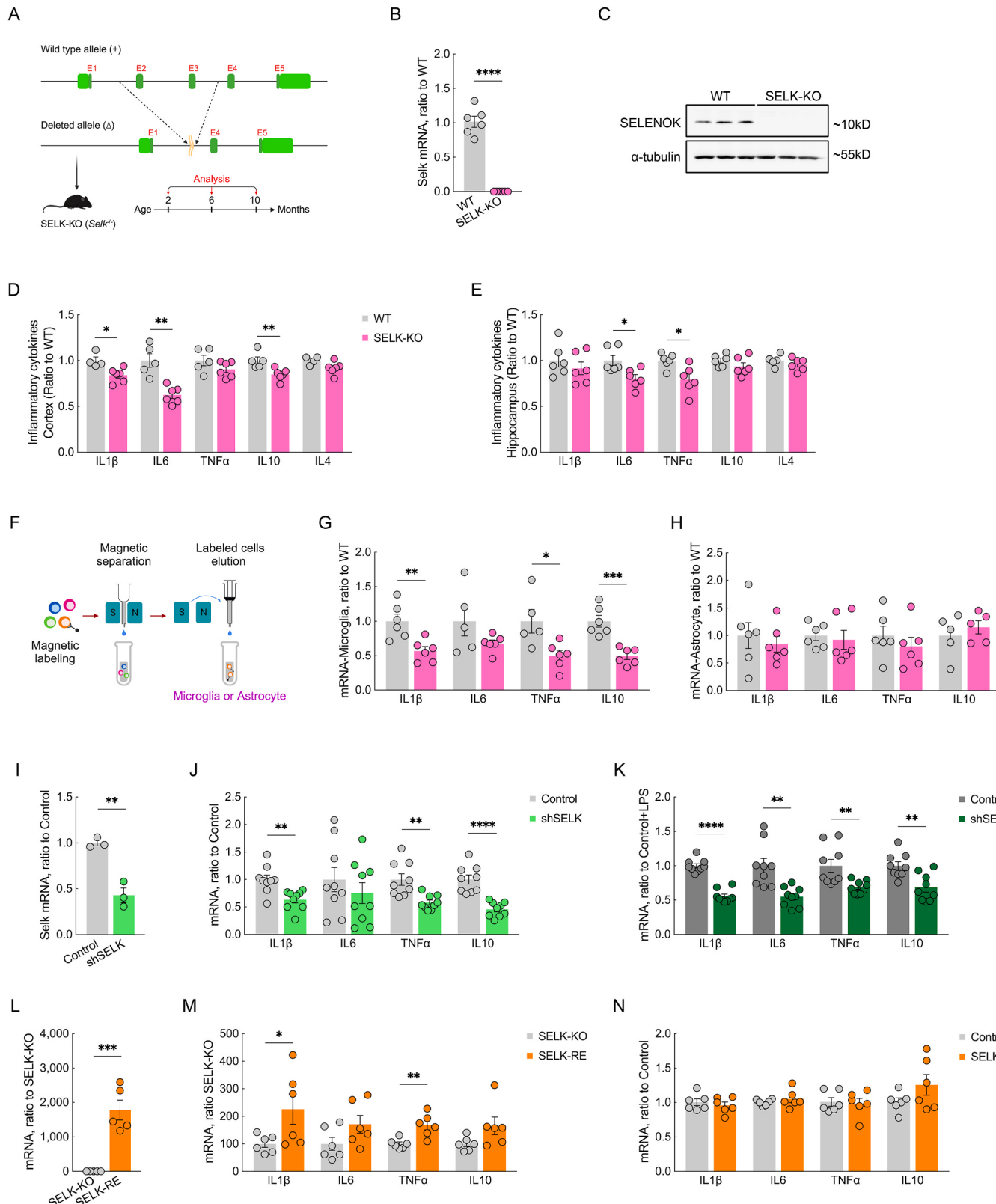
#### 2.19. Statistical analysis

All data were analyzed with GraphPad Prism 9 (GraphPad Software, La Jolla, CA, USA) and presented as the mean ± SEM (\*p < 0.05, \*\*p < 0.01, \*\*\*p < 0.001, and \*\*\*\*p < 0.0001). Experimental comparisons were performed using ANOVA, followed by the appropriate post hoc test, or with an unpaired Student’s t-test. The statistical method used for each quantitated data, as well as the specific sample sizes, are described in relevant figure legends.

### 3. Results

#### 3.1. SELENOK depletion impairs the microglial immune response

To confirm the impact of SELENOK on brain immune homeostasis,



(caption on next page)

**Fig. 1.** SELENOK regulates inflammatory cytokine levels in microglia.

(A) Schematic diagram showing the wild-type (WT) and mutant SELENOK alleles and age of experimental SELENOK knockout (SELK-KO) mice. (B–C) Levels of SELENOK (B) mRNA ( $n = 6$ ) and (C) protein ( $n = 3$ ) in SELK-KO mice. (D–E) Levels of inflammatory cytokines (pro-inflammatory factors: IL-1 $\beta$ , IL-6, TNF- $\alpha$ ; anti-inflammatory factors: IL-10 and IL-4) were assessed using ELISA in (D) cortical and (E) hippocampal samples from 10-month-old wild-type and SELK-KO mice ( $n = 6$  per group; 3 male and 3 female mice). (F) Cartoon showing the isolation of single cells from the whole brains of 10-month-old WT and SELK-KO mice for magnetic bead sorting of microglia. (G–H) Gene expression of inflammatory cytokines in (G) adult microglia and (H) astrocytes ( $n = 6$  per group; 3 male and 3 female mice). (I) The mRNA levels of SELENOK in SELENOK knockdown (shSELK; via adenovirus transfection) primary microglia from WT mice ( $n = 3$  independent experiments; three replicates). (J) Gene expression of inflammatory cytokines (IL-1 $\beta$ , IL-6, TNF- $\alpha$ , and IL-10) was assessed in control and shSELK primary microglia ( $n = 3$  independent experiments; three replicates). (K) Gene expression of inflammatory cytokines was assessed in LPS-treated control and shSELK primary microglia ( $n = 3$  independent experiments; three replicates). (L) SELENOK mRNA levels after SELENOK re-expression (SELK-RE; via adenovirus transfection) in mice with SELK-KO primary microglia ( $n = 3$  independent experiments; two replicates). (M) Gene expression of inflammatory cytokines in SELK-KO and SELK-RE primary microglia ( $n = 3$  independent experiments; two replicates). (N) Gene expression of inflammatory cytokines in control and SELENOK overexpressing (SELK-OE; via adenovirus transfection) HMC3 cells ( $n = 3$  independent experiments; two replicates). All data are presented as the mean  $\pm$  SEM and analyzed using Student's t-test. \* $p < 0.05$ ; \*\* $p < 0.01$ ; \*\*\* $p < 0.001$ ; \*\*\*\* $p < 0.0001$ .

SELK-KO mice were generated using the CRISPR-Cas9 system, as shown in Fig. 1A–C. Longitudinal ELISA assessments of inflammatory cytokines (pro-inflammatory factors: IL-1 $\beta$ , IL-6, and TNF- $\alpha$ ; anti-inflammatory factors: IL-10 and IL-4) revealed no significant changes in the brains of WT and SELK-KO mice at two and six months of age (Fig. S1). However, at 10 months, a significant decrease was observed in the cortical levels of IL-1 $\beta$ , IL-6, and IL-10, as well as the hippocampal levels of IL-6 and TNF- $\alpha$  (Fig. 1D and E).

Glial cells are a predominant source of brain inflammatory cytokines. Hence, we isolated microglia and astrocytes from adult mouse brains using magnetic bead antibodies (Fig. 1F). A notable downregulation in IL-1 $\beta$ , TNF- $\alpha$ , and IL-10 transcription was detected in SELK-KO microglia relative to their WT counterparts (Fig. 1G), aligning with the brain inflammatory cytokine profiles. In contrast, the levels of these cytokines in astrocytes of WT and SELK-KO mice showed no significant differences (Fig. 1H), implicating microglia as the primary locus of cytokine dysregulation in the SELK-KO mouse brain.

Next, we constructed shSELK primary microglia using adenoviral vectors (Fig. 1I). The shSELK microglia had substantially reduced IL-1 $\beta$ , TNF- $\alpha$ , and IL-10 mRNA levels (Fig. 1J). Similarly, the knockdown of SELENOK in HMC3 cells (Figs. S2A–C) resulted in a significant decrease in the expression levels of IL-1 $\beta$ , IL-6, TNF- $\alpha$ , and IL-10 (Fig. S2D). These results suggest that the reduction in inflammatory cytokine levels caused by SELK-KO or shSELK may affect microglial activation. To further test the immune response of microglia to extracellular stimuli, we treated them with LPS. Following LPS treatment, both primary microglia and HMC3 cells exhibited a significant increase in inflammatory cytokine expression (Figs. S2E–F). However, in shSELK primary microglia and HMC3 cells, these levels were significantly lower than those in the controls (Fig. 1K and S2G), a result indicative of dampened immune activation by microglia due to a SELENOK deficit. Subsequent re-expression of SELENOK (SELK-RE) in SELK-KO primary microglia (Fig. 1L) led to a significant increase in IL-1 $\beta$  and TNF- $\alpha$  levels (Fig. 1M). However, SELK-OE in HMC3 cells (Figs. S2F–H) did not increase the cytokine expression levels (Fig. 1N). These findings suggest that SELENOK expression helps maintain microglial immune homeostasis.

### 3.2. SELENOK regulates microglial migration and phagocytosis

Microglial proliferation is crucial for central nervous system immune homeostasis [41]. Alterations in SELENOK levels in HMC3 cells did not affect cell proliferation (Fig. S3A). Consistent with these in vitro findings, no significant differences were observed in the levels of IBA1 $^+$  microglia (an immunohistochemical marker for both ramified and activated microglia) in vivo between 10-month-old mice in the SELK-KO and WT groups (Fig. S3B). Moreover, flow cytometric analysis of the CD11b $^+$ /CD45 $^{\text{low}}$  microglial subset within brain single-cell suspensions indicated no substantial variance in microglial proportions between the two groups (Fig. 2A), further suggesting the non-involvement of SELENOK in regulating microglial proliferation and density.

Microglial activation is involved in the regulation of its functionality,

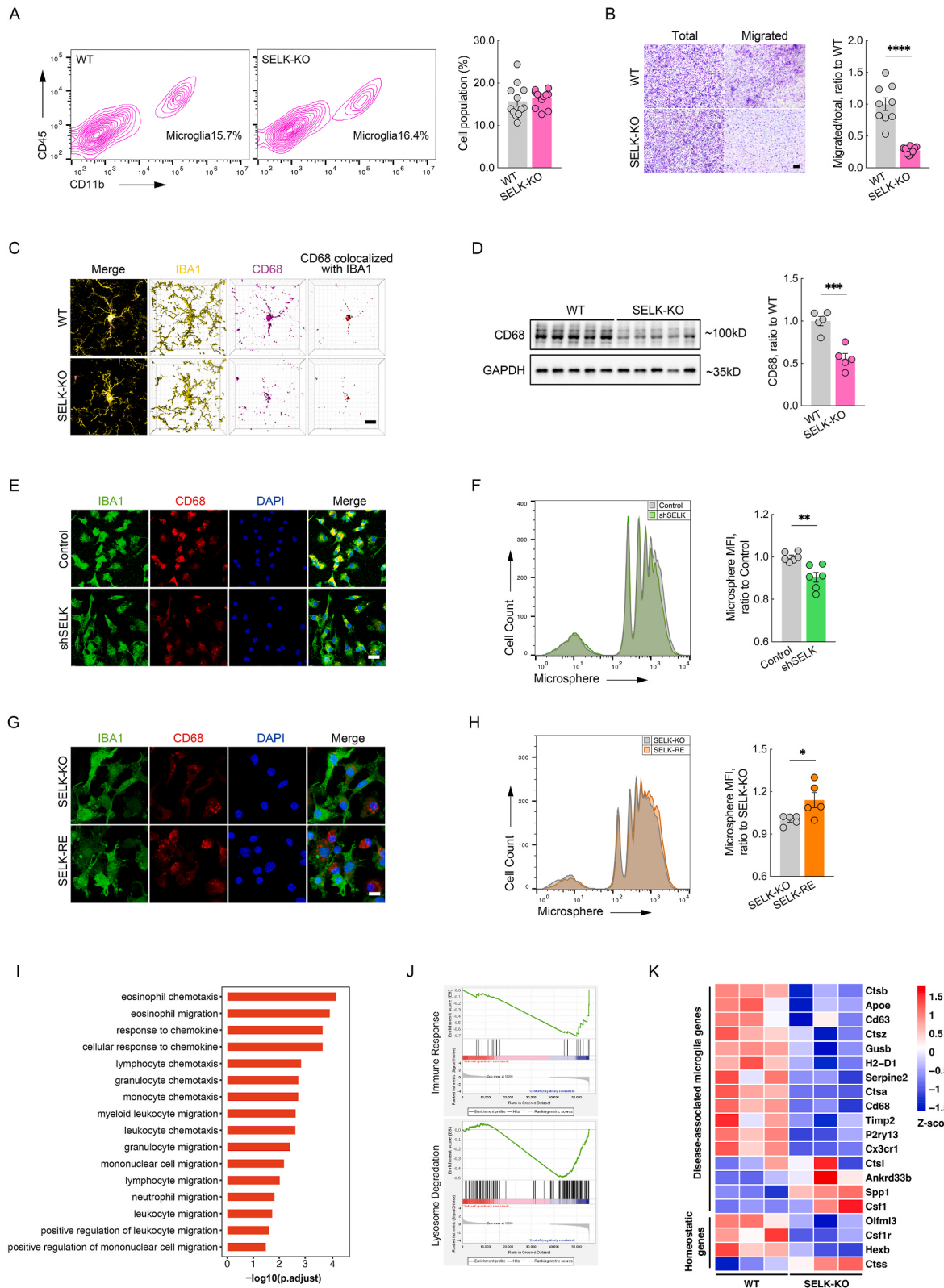
and SELENOK deficiency is linked to compromised microglial activation [42]. Although SELENOK has been reported to modulate BV2 cell migration and phagocytosis in vitro [43], a de novo evaluation of its effects on microglial functions in vivo is warranted. Microglial migration, a prerequisite for efficacious immune surveillance and response, was examined using a transwell migration assay. SELK-KO primary microglia exhibited significantly reduced migration compared to that of WT cells (Fig. 2B and S3C). In HMC3 cells, shSELK further corroborated this migratory impairment (Figs. S4A–B), indicating that a deficiency in SELENOK expression impairs microglial migration.

Microglial immunity mainly relies on their phagocytic activity. CD68 is a highly glycosylated transmembrane protein whose levels are upregulated in actively phagocytosing microglia and monocytes, serving as a marker of microglial phagocytic activity in microglia [32,44]. CD68 colocalization in the brain microglia of 10-month-old SELK-KO mice was reduced based on immunofluorescence combined with 3D reconstruction (Fig. 2C) and quantitative western blotting analysis (Fig. 2D). Similarly, in both primary microglia and HMC3 cells in vitro, CD68 expression was significantly reduced in shSELK microglia, as detected by immunofluorescence and western blotting analysis (Fig. 2E and S4C–E).

To characterize microglial phagocytosis more directly, fluorescent microspheres (1  $\mu\text{m}$  diameter) were co-incubated with microglia and cultured for 3 h. Flow cytometric analysis showed that shSELK significantly reduced microsphere fluorescence within both primary microglia and HMC3 cells (Fig. 2F and S4F–G); and in shSELK HMC3 cells, the proportion of cells capable of phagocytosing microspheres was also significantly reduced (Figs. S4H–I). Conversely, SELK-RE in SELK-KO primary microglia significantly augmented CD68 expression and phagocytic capacity (Fig. 2G and H). Importantly, astrocytic phagocytosis appeared unaffected by SELENOK manipulation, highlighting a microglia-specific regulatory role of SELENOK in the brain (Figs. S3D–F).

To further understand the role of SELENOK in microglial function, adult mouse microglia RNA was sequenced. RNA-seq analysis revealed that 317 genes were differentially expressed in SELK-KO microglia compared to that in the WT group: 203 upregulated and 114 downregulated ( $|\log_2(\text{FC})| > 1$  and  $p < 0.05$ ) (Figs. S5A–B). Clustering analysis underscored distinct expression patterns in the two groups (Fig. S5C). GO-biological process analysis revealed that the downregulated genes notably enriched pathways linked to immune cell migration (Fig. 2I). The GSEA indicated significant enrichment of these genes in negative regulatory pathways of immune response and lysosomal degradation (Fig. 2J), highlighting the impact of SELK-KO on microglial activation, migration, and phagocytosis. However, the scattered distribution of these differential genes across the GO and KEGG pathways suggests that the RNA-seq data, while informative, falls short in pinpointing clear molecular targets or mechanisms underlying the effects of SELENOK on microglia.

Disease-associated microglia (DAM), a subtype of microglia identified via single-cell RNA-seq, is pivotal in  $\text{A}\beta$  phagocytosis and AD pathology [45]. Except for homeostatic genes (*Csf1r*, *Hexb*, etc.), the



(caption on next page)

**Fig. 2.** SELENOK modulates microglial migration and phagocytosis without impacting microglial proliferation. (A) Representative flow plots and population analysis of FACS-sorted CD45/CD11b<sup>+</sup> microglia from brain samples of 10-month-old wild-type (WT) and SELENOK knockout (SELK-KO) mice (n = 6 per group; 3 male and 3 female mice). (B) Migration of primary microglia and its quantifications in WT and SELK-KO mice. (n = 3 independent experiments; three regions). (C) Representative 3D reconstruction and rendering of CD68 signals inside Iba1-positive microglia from WT and SELK-KO mice at 10 months using Imaris software Bar = 5 μm. (D) Representative CD68 immunoblots and their quantification in cortical lysates of WT and SELK-KO mice (n = 5 per group; 3 male and 2 female mice). (E) Representative Iba1 (green), CD68 (red), and DAPI (blue) immunofluorescence in control and SELENOK knockdown (shSELK) primary microglia. Bar = 10 μm. (F) Flow cytometric analysis of phagocytosis in control and shSELK primary microglia. Representative histograms and summary bar graphs showing the frequencies of cells containing fluorescent microspheres (n = 3 independent experiments; two replicates). (G) Representative images showing Iba1 (green), CD68 (red), and DAPI (blue) immunofluorescence in SELK-KO and SELENOK re-expression (SELK-RE) primary microglia. Bar = 10 μm. (H) Flow cytometric analysis of phagocytosis in SELK-KO and SELK-RE primary microglia. Representative histograms and summary bar graphs showing the frequencies of cells containing fluorescent microspheres (n = 3 independent experiments; two replicates). (I) Gene ontology (biological process) analysis of the 114 downregulated genes in the WT versus SELK-KO microglia (|log2(FC)| > 1 and q < 0.05). (J) Gene set enrichment analyses (GSEA) of differentially expressed genes (DEGs) related to immune response (NES = -1.33, FDR < 0.01) and lysosome degradation (NES = -1.28, FDR < 0.01) in WT versus SELK-KO microglia. NES: normalized enrichment score; FDR: false discovery rate. (K) Clustering expression heatmap of disease-associated microglia-related DEGs (FPKM, p < 0.01) from RNA-seq analysis of the microglia of 10-month-old WT and SELK-KO mice (Z-score) (n = 3 per group; 2 male and 1 female mice). All data are presented as the mean ± SEM and analyzed via Student's t-test. \*p < 0.05; \*\*p < 0.01; \*\*\*p < 0.001; \*\*\*\*p < 0.0001. (For interpretation of the references to colour in this figure legend, the reader is referred to the Web version of this article.)

transition from homeostatic to DAM microglia, as regulated by key genes and marked by the upregulation (*ApoE*, *Ctsb*, *H2-D1*, *Tim2* in stage 1 DAM, and *Spp1*, *Axl*, *Cd68*, *Cd6s*, and *Gusb* in stage 2 DAM) or downregulation (*P2ry13* and *Cx3cr1*) of genes, emerged as a potential therapeutic pathway in AD treatment [45–47]. We further analyzed the RNA-seq data based on FPKM values, leading to the identification of a comprehensive differential gene expression profile in SELK-KO microglia (p < 0.01). A comparison of gene expression profiles between SELK-KO microglia and DAM intriguingly revealed a downregulation in most key genes facilitating this transition in SELK-KO microglia (Fig. 2K). This deviation from the DAM phenotype in SELK-KO microglia leads to speculation of the critical role that SELENOK-induced microglial dysfunction plays in the process of Aβ phagocytosis and deposition in AD. In addition, the observed alterations in expression of these homeostatic genes, including *Csf1r*, *Hexb*, *Olfml3*, and *Ctss*, further corroborate that the knockout of SELENOK induces a disruption in the fundamental immune functions of microglia.

### 3.3. SELENOK promotes microglial phagocytosis and clearance of Aβ

The above data confirmed that SELENOK significantly regulates microglial function, suggesting a potential impact on microglial Aβ phagocytosis. Primary microglia co-incubated with fluorescent-labeled Aβ<sub>42</sub> oligomers (FAM-Aβ<sub>42</sub>) showed significantly reduced FAM-Aβ<sub>42</sub> phagocytosis in shSELK cells (Fig. 3A), as corroborated through flow cytometry quantification, which showed reduced Aβ fluorescence following SELK-KO (Fig. 3B). Similarly, shSELK HMC3 cells displayed reduced FAM-Aβ<sub>42</sub> uptake (Figs. S6A–B). Conversely, SELK-RE in SELK-KO primary microglia significantly increased FAM-Aβ<sub>42</sub> phagocytosis (Fig. 3C and D), which was also observed in SELK-OE HMC3 cells when compared to that in the controls (Figs. S6C–D). Notably, SELK-KO did not affect FAM-Aβ<sub>42</sub> phagocytosis in primary astrocytes (Figs. S6E–F), indicating a microglia-specific role.

Aβ phagocytosed by microglia is transported to lysosomes for degradation and clearance. Following post-Aβ<sub>42</sub> oligomer co-incubation, Aβ degradation was further assessed in primary microglia in the presence and absence of lysosomal enzyme inhibitors (pepstatin A, leupeptin, and E-64d) and chloroquine. Cell-associated Aβ<sub>42</sub> levels were significantly lower in shSELK microglia exposed to lysosomal inhibitors (Fig. 3E), but no notable changes were observed without inhibitor treatment (Fig. 3F). Calculation of the Aβ degradation rate (subtracting Aβ<sub>42</sub> levels in the absence of inhibitors from that in the presence of inhibitors) revealed a significant reduction in Aβ<sub>42</sub> degradation in shSELK microglia (Fig. 3F). In SELK-KO microglia, SELK-RE following chloroquine treatment significantly increased cell-associated Aβ<sub>42</sub> levels (Fig. 3G), and Aβ degradation was significantly enhanced in SELK-RE microglia (Fig. 3H). This suggests that SELENOK also affects microglial Aβ degradation.

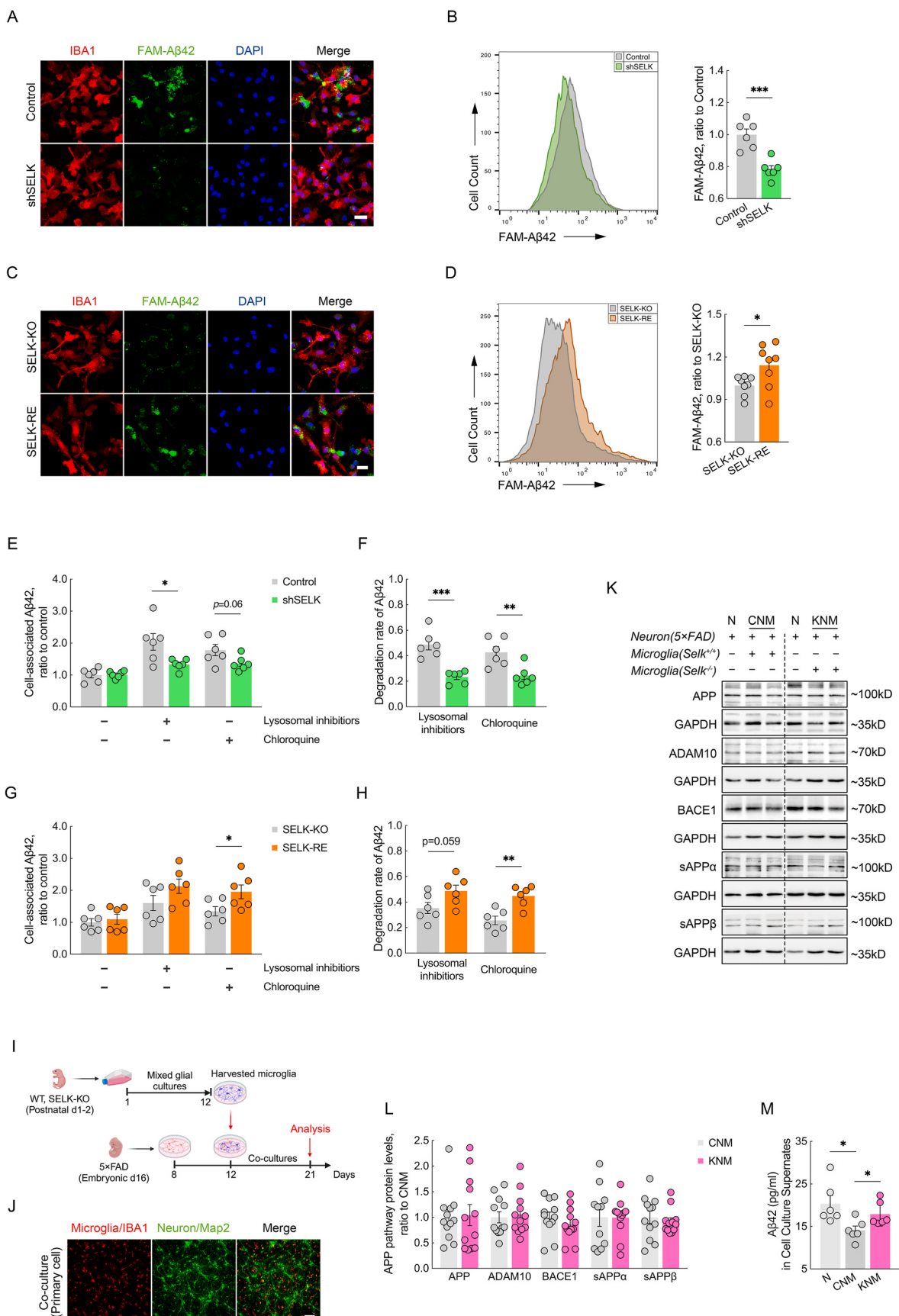
To further confirm the impact of SELENOK on the microglial phagocytosis of neuronal Aβ (derived from human APP transgenes), primary neurons from AD-transgenic mice (5xFAD) were co-cultured with WT (CNM), and SELK-KO (KNM) primary microglia (Fig. 3I and J). In this co-culture system, Aβ levels in the medium primarily depended on its production by AD neurons and phagocytosis by microglia. The Aβ production pathway analysis showed no differences in cleavage enzymes (ADAM10 and BACE1) or their products (sAPPα and sAPPβ) in the CNM and KNM co-cultures (Fig. 3K–L), indicating comparable Aβ production. Compared to those in AD neurons cultured alone (N), the CNM co-cultures showed significantly lower Aβ<sub>42</sub> levels in the medium, indicative of the microglial phagocytosis ability of microglia in the co-culture system (Fig. 3M). Interestingly, compared to those of CNM, the KNM co-culture had significantly higher Aβ<sub>42</sub> levels in the medium (Fig. 3M), suggesting that SELK-KO markedly inhibits microglial phagocytosis of neuronal Aβ.

### 3.4. SELENOK knockout inhibits microglial Aβ phagocytosis and aggravates cognitive impairment in AD mice

To investigate the impact of SELENOK on microglial Aβ phagocytosis in vivo, a SELK-KO model was developed in 5xFAD mice (AD-SELK-KO; a whole-body SELK deletion AD model) (Fig. 4A and S7A). Morris water maze assessments of 10-month-old mice demonstrated a significantly increased escape latency on training Day 4 in AD-SELK-KO mice compared to that in AD mice (Fig. 4B). The AD-SELK-KO mice also showed a notable decrease in time spent in the target quadrant during a probe trial 24 h post-training (Fig. 4C). Based on consistent swimming speeds across all mice groups (Fig. 4D), motor function deficits were excluded.

Subsequent brain analysis of AD-SELK-KO mice revealed a significant increase in Aβ plaque accumulation in the cortex and hippocampus (Fig. 4E). ELISA quantification confirmed elevated RIPA-soluble Aβ levels in these brain regions following SELK-KO (Fig. 4F and G), which is suggestive of an intensified Aβ pathology. High-magnification imaging of mouse brain tissue sections revealed a notable reduction in microglia near Aβ plaques in the hippocampus and cortex of AD-SELK-KO mice compared to that in AD mice (Fig. 4H and I). For a quantitative insight into microglial Aβ phagocytosis in vivo, methoxy-X04 was employed as a fluorescent Aβ marker, followed by flow cytometric analysis of brain single-cell suspensions. The WT and SELK-KO mice had a negligible presence of methoxy-X04-positive microglia. AD-SELK-KO mice showed a pronounced decrease in methoxy-X04<sup>+</sup>CD11b<sup>+</sup>CD45<sup>low</sup> microglial populations compared to that in AD mice (Fig. 4J and K), indicating diminished Aβ phagocytosis in microglia due to SELK-KO.

Given the multifaceted factors affecting brain Aβ levels, including its production, degradation pathways in neurons, degrading enzymes, and microglial phagocytic degradation, further investigations were



(caption on next page)

**Fig. 3.** Effects of SELENOK on microglial phagocytosis and clearance of A $\beta$  in vitro.

(A) Representative fluorescence micrographs illustrating phagocytosis of carboxyfluorescein-A $\beta$ 42 (FAM-A $\beta$ 42; green) in control and SELENOK knockout (shSELK) primary microglia stained with Iba1 (red) and DAPI (blue). Bar = 10  $\mu$ m. (B) Flow cytometric analysis of A $\beta$  phagocytosis in control and shSELK primary microglia. Representative histogram and summary bar graphs showing frequencies of the cells containing FAM-A $\beta$ 42 ( $n = 6$  independent experiments). (C) Representative fluorescence micrographs illustrating phagocytosis of FAM-A $\beta$ 42 (green) in SELENOK knockout (SELK-KO) and SELENOK re-expression (SELK-RE) primary microglia stained with Iba1 (red) and DAPI (blue). Bar = 10  $\mu$ m. (D) Flow cytometric analysis of A $\beta$  phagocytosis in SELK-KO and SELK-RE primary microglia. Representative histogram and summary bar graphs showing frequencies of the cells containing FAM-A $\beta$ 42 ( $n = 4$  independent experiments; two replicates). (E, G) Quantification of cell-associated A $\beta$ 42 in control, shSELK, SELK-KO, and SELK-RE primary microglia using ELISA ( $n = 3$  independent experiments, two replicates). (F, H) Amounts of degraded A $\beta$ 42 were calculated by subtracting the cell-associated A $\beta$ 42 in the absence of inhibitors from that in the presence of inhibitors ( $n = 3$  independent experiments; two replicates). (I) Schematic diagram of the primary microglia and neuron co-culture system. (J) Representative immunofluorescence of co-cultured primary microglia and neurons stained with Iba1 (red) and Map2 (green). Bar = 100  $\mu$ m. (K) Quantification of human A $\beta$ 42 levels in the co-culture supernatants using ELISA ( $n = 6$  independent experiments). (L–M) Representative immunoblots and quantifications of APP, ADAM10, BACE1, sAPP $\alpha$ , and sAPP $\beta$  protein expression levels in cell lysates from the co-culture system ( $n = 6$  independent experiments; two replicates). C: AD primary neurons; CNM: AD primary neurons co-cultured with WT primary microglia; KNM: AD primary neurons co-cultured with SELK-KO primary microglia. All data are presented as the mean  $\pm$  SEM and analyzed via Student's t-test. \* $p < 0.05$ ; \*\* $p < 0.01$ ; \*\*\* $p < 0.001$ . (For interpretation of the references to colour in this figure legend, the reader is referred to the Web version of this article.)

conducted. Analysis of A $\beta$  production pathways in mouse brains post-SELK-KO showed no significant changes in the levels of APP, ADAM10, BACE1, sAPP $\alpha$ , and sAPP $\beta$  (Figs. S7B–C). Similar results were obtained from in vitro studies with AD primary neurons (Figs. S7B–D). ELISA analysis further confirmed stable neuronal A $\beta$  levels following SELK-KO (Fig. S7E), indicating that SELENOK likely does not affect neuronal A $\beta$  production. Additionally, quantitative PCR of key A $\beta$ -degrading enzymes (insulin-degrading enzyme, neprilysin, endothelin-converting enzyme 1, and matrix metalloproteinase 2) in the mouse brain showed no significant alterations between the two groups (Fig. S7F). These findings collectively suggest that the elevated A $\beta$  levels in AD-SELK-KO mouse brains are primarily attributed to reduced microglial A $\beta$  phagocytosis caused by SELK-KO.

### 3.5. SELENOK overexpression in microglia enhances A $\beta$ phagocytosis and improves cognitive deficits in AD mice

Addressing the challenge of effectively labeling and manipulating microglia, the novel AAV-MG1.2 vector, recently developed by Luo et al., coupled with a Cre-dependent reporter system, has facilitated gene modifications within microglia [48]. Using the Cre/loxP system, heterozygous Cx3cr1<sup>CreER</sup>-5xFAD mice were generated (Fig. 5A). Following AAV vector administration and subsequent tamoxifen induction in eight-week-old mice, IBA1 immunostaining verified targeted microglial infection, and significant upregulation of SELENOK expression in the cortex and hippocampus was observed (Fig. 5B and C), confirming SELK-OE in microglia of the AD mouse brain.

Behavioral and pathological assessments were conducted 23 weeks post-viral injection. In the Morris water maze, SELK-OE significantly reduced escape latency in AD mice and increased time spent in the target quadrant during a 24-h probe trial without affecting motor abilities (Fig. 5D–F), signifying an improvement in cognitive deficits. Further immunofluorescence staining and ELISA quantification showed a notable reduction in A $\beta$  plaque count in the targeted cortical and hippocampal regions (Fig. 5G). Additionally, there was a significant decrease in RIPA- and SDS-soluble A $\beta$  levels in the brains of SELK-OE AD mice (Fig. 5H). Crucially, an increased number of microglia surrounding A $\beta$  plaques in the cortex and hippocampus (Fig. 5I) and a higher proportion of methoxy-X04<sup>+</sup>CD11b<sup>+</sup>CD45<sup>low</sup> cells (Fig. 5J) were detected. Hence, overexpression of SELENOK in microglia significantly enhances A $\beta$  phagocytosis in the brains of AD mice.

### 3.6. SELENOK-dependent CD36 palmitoylation modulates microglial function and A $\beta$ phagocytosis

The above findings demonstrate the role that SELENOK plays in modulating microglial A $\beta$  phagocytosis and AD progression and establish links between SELENOK and microglial function. However, the mechanisms governing its impact on microglia remain unclear. As no

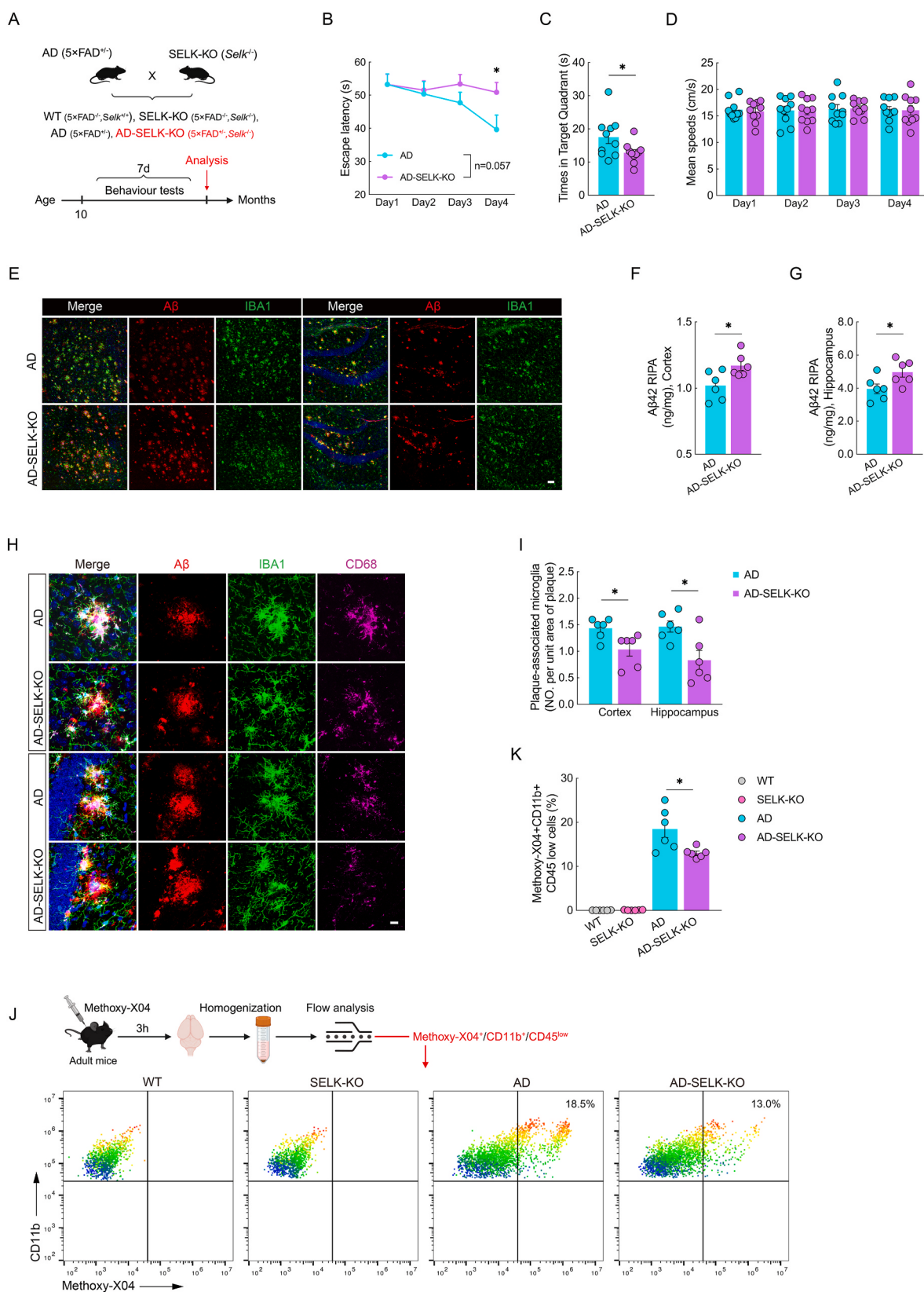
direct and effective targets or mechanisms were identified at the transcriptomic level, we shifted our focus to exploring the mechanisms from the perspective of microglial A $\beta$  phagocytosis. Microglial A $\beta$  phagocytosis is reliant on specific receptors [49–53], including CD36, which is not only a critical A $\beta$  receptor but also a palmitoylated protein modulated by SELENOK [54,55]. However, this has been shown only in macrophages, with no direct evidence of the regulation of CD36 palmitoylation by SELENOK in the microglia or brain.

We found that while SELK-KO did not alter CD36 expression, it significantly reduced CD36 palmitoylation (Fig. 6A). This finding was further confirmed in primary microglia and HMC3 cells, where CD36 palmitoylation significantly decreased in shSELK cells and increased in SELK-OE cells (Fig. 6B and S8A–B). Moreover, microglial CD36 transcription showed no significant differences between controls and SELK-KO or shSELK cells (Figs. S8C–D), indicating that SELENOK regulates the post-translational modification, namely palmitoylation, of CD36 in microglia.

Studies by Hoffmann et al. have shown that SELENOK interacts with the ER-located palmitoyltransferase, DHHC6, enhancing its catalytic efficiency in palmitoylation [56–58]. We knocked down DHHC6 in HMC3 cells (shDHHC6) to confirm its involvement in the SELENOK-mediated modulation of CD36 palmitoylation, and found a significant reduction in CD36 palmitoylation (Fig. 6C and D). However, overexpression of SELENOK in shDHHC6 cells no longer affected CD36 palmitoylation (Fig. 6C and D), indicating that SELENOK affects CD36 palmitoylation via DHHC6. Conversely, overexpressing DHHC6 in microglia naturally increased CD36 palmitoylation, which was significantly reduced in response to shSELK (Figs. S8E–F). These findings demonstrate that the efficacy of the palmitoylation system, given adequate DHHC6 expression, is predominantly reliant on SELENOK.

Given the impact of SELENOK on CD36 palmitoylation in microglia, we next explored its involvement in microglial A $\beta$  phagocytosis. Based on reported palmitoylation sites in CD36 (Cys3, Cys7, Cys464, and Cys466), we overexpressed WT CD36 and a palmitoylation site mutant (C3S, C7S, C464S, and C466S) (SSSS) in HMC3 cells (Fig. S9A). DHHC6 knockdown (DHHC6-KD) significantly impaired microglial A $\beta$  phagocytosis in the WT cells (Figs. S9B–C), whereas in SSSS cells, DHHC6-KD no longer affect this process (Figs. S9D–E), indicating that CD36 palmitoylation directly influences microglial A $\beta$  phagocytosis. Additional experiments with these cell models confirmed that changes in SELENOK expression levels affected microglial A $\beta$  phagocytosis in WT cells (Fig. 6E and F), but not in SSSS cells (Fig. 6G). These findings demonstrate the dependence of SELENOK on CD36 palmitoylation for regulating microglial A $\beta$  phagocytosis.

We further explored whether the regulation of microglial functions by SELENOK extends to non-AD conditions through CD36 palmitoylation. Overexpressing WT CD36 in HMC3 cells enhanced microglial migration and phagocytosis, whereas these capabilities were significantly reduced in the SSSS mutants, directly linking CD36



(caption on next page)

**Fig. 4.** SELENOK knockout impairs microglial A $\beta$  phagocytosis and aggravates AD pathology in vivo.

(A) Schematic diagram for generating SELENOK-knockout 5xFAD mice (AD-SELK-KO; a whole-body SELK deletion AD model) and experimental timetable. (B–D) Morris water maze tests were performed with 10-month-old 5  $\times$  FAD (AD) and AD-SELK-KO mice ( $n = 10$  per group; 5 male and 5 female mice). (B) Escape latency time to reach the hidden platform was recorded during the 4-day training. (C) A probe trial was performed 24 h after the last trial of a hidden platform task, and the search time for the target quadrant recorded. (D) Swimming speeds of the two groups were recorded during the tests. (E) Representative immunofluorescence of coronal sections from AD and AD-SELK-KO mice stained with Iba1 (green), MOAB-2 (A $\beta$ , red), and DAPI (blue). Bar = 50  $\mu$ m. (F–G) Quantification of human A $\beta$ 42 levels (RIPA-soluble) in the cortical (F) and hippocampal (G) samples from 10-month-old AD and AD-SELK-KO mice using ELISA ( $n = 6$  per group; 3 male and 3 female mice). (H) Magnified view of (E). Representative immunofluorescence of A $\beta$  plaques and microglia from AD and AD-SELK-KO mice stained with Iba1 (green), MOAB-2 (A $\beta$ , red), CD68 (purple), and DAPI (blue). Bar = 20  $\mu$ m. (I) Number of A $\beta$  plaque-associated microglia in (H) ( $n = 3$  per group; six sections; 30 A $\beta$  plaques). (J) Representative FACS dot plots showing the microglial phagocytosis of A $\beta$  in WT, SELK-KO, AD, and AD-SELK-KO mice. (K) Percent (%) methoxy-X04 $^+$ CD11b $^+$ CD45 $^{low}$  microglia determined through flow cytometry isolated from the brain of the four groups of mice indicated in (J) ( $n = 6$  per group; 3 male and 3 female mice). All data are presented as the mean  $\pm$  SEM. Data from (B) were analyzed via two-way ANOVA and Bonferroni post hoc analyses. Student's t-test was used to analyze the other data. \* $p < 0.05$ ; \*\* $p < 0.01$ ; \*\*\* $p < 0.001$ . (For interpretation of the references to colour in this figure legend, the reader is referred to the Web version of this article.)

palmitoylation to microglial functionality (Fig. 6H–J). Collectively, these findings establish CD36 palmitoylation as a direct target through which SELENOK modulates microglial functions and A $\beta$  phagocytosis.

### 3.7. SELENOK facilitates CD36 localization to microglial plasma membranes through palmitoylation regulation

CD36 palmitoylation has been linked to microglial functions and A $\beta$  phagocytosis. Yet, further understanding of how this palmitoylation influences microglial A $\beta$  phagocytosis remains essential to fully elucidate the regulatory role of SELENOK in microglia. Palmitoylation typically governs protein transport and membrane localization and plays a pivotal role in CD36 functionality [59,60]. Previous studies indicate that palmitoylation assists CD36 in localizing within the cellular membrane system, facilitating its transport to the cell membrane [54,61]. Evidently, CD36 localization in the microglial membrane is crucial for it to recognize and bind A $\beta$ , thus enhancing microglial phagocytosis and A $\beta$  degradation [62]. Therefore, the impact of CD36 palmitoylation on its localization and expression on the microglial surface was further confirmed. Compared to that in WT cells, SSSS cells had significantly lower CD36 expression in the cell membrane (Fig. 7A and B). Additionally, either knocking down or overexpressing DHHC6 in WT cells significantly lowered or raised microglial surface CD36 expression, respectively (Fig. 7C), indicating the direct role of CD36 palmitoylation in its membrane surface presence.

Further analysis focused on the effect of SELENOK on CD36 expression in microglial membranes. Flow cytometric analysis of single-cell suspensions from adult mouse brains revealed notably lower CD36 levels in SELK-KO microglial membranes (Fig. 7D). Similarly, in WT primary microglia, SELENOK levels corresponded directly with the CD36 membrane expression levels (Fig. 7E and F). Additionally, a significant decrease in surface CD36 expression was observed in cultured SELK-KO primary microglia compared to that in the WT counterparts (Fig. 7G and H). These findings, both *in vivo* and *in vitro*, highlight the pivotal role that SELENOK plays in modulating CD36 expression in microglial membranes and, consequently, microglial A $\beta$  phagocytosis. Changes in SELENOK expression affected CD36 membrane expression in WT but not in SSSS models of HMC3 cells (Fig. 7I–K), demonstrating that its regulatory effect on microglial membrane CD36 levels is dependent on CD36 palmitoylation.

### 3.8. Se supplementation elevates reduced CD36 palmitoylation levels and enhances microglial A $\beta$ phagocytosis in AD

We have previously shown a notable decline in SELENOK levels in the brains of patients with AD [23]. Theoretically, this suggests that pathological changes associated with a SELENOK deficit, such as reduced CD36 palmitoylation (seen in SELK-KO microglia), might also occur in AD. Confirming this hypothesis, 5xFAD mouse brains showed significantly reduced levels of SELENOK and CD36 palmitoylation and increased levels of total CD36, but no discernible changes in DHHC6

levels (Fig. 8A). Flow cytometry of adult mouse brain microglia also indicated a significant decrease in CD36 levels in AD microglial membranes (Fig. 8B). Importantly, similar findings were observed in human AD brains, with decreased SELENOK expression and CD36 palmitoylation (Fig. 8C and D). These results suggest that impaired CD36 palmitoylation, leading to reduced microglial A $\beta$  phagocytosis, is involved in AD progression. Enhancing CD36 palmitoylation could, therefore, potentially augment microglial A $\beta$  phagocytosis, identifying a key mechanism by which SELK-OE could mitigate AD.

A key aim in studying the relationship between SELENOK and AD is to explore the systemic mechanisms underlying Se-mediated prevention of AD. Therefore, we next explored whether SELENOK-mediated CD36 palmitoylation, which affects microglial A $\beta$  phagocytosis, is a crucial mechanism in the anti-AD effects of Se. *In vitro*, treatment of primary microglia with SeM and SeNa significantly elevated SELENOK levels and promoted CD36 palmitoylation without altering CD36 expression (Fig. 8E and F). Further functional assays showed that Se supplementation significantly increased microglial membrane CD36 levels and its A $\beta$  phagocytosis (Fig. 8G and H), indicating that Se potentially boosts microglial A $\beta$  phagocytosis via the CD36 palmitoylation pathway.

*In vivo* experiments involving an 8-week intraperitoneal injection of SeM and SeNa in 5xFAD mice (Fig. 8I) resulted in a significant upregulation of SELENOK expression in mouse brains (Fig. 8J). A notable reduction was observed in A $\beta$  plaque counts in the hippocampus and cortex of these mice (Fig. 8K). Moreover, both Se compounds significantly increased CD36 palmitoylation in mouse brains without affecting total CD36 expression (Fig. 8L–M). Additionally, SeM and SeNa markedly increased the number of A $\beta$  plaques associated with microglia (Fig. 8N), suggesting that Se supplementation enhances microglial A $\beta$  phagocytosis in AD mouse brains. Therefore, our study substantiates that SELENOK-mediated microglial functions are pivotal mechanisms in the anti-AD effects of Se.

## 4. Discussion

Immune regulation, a critical biological function of Se, engages various selenoproteins [63,64], of which SELENOK is a key immune regulator [35,37]. SELENOK deficiency hinders the proliferation, differentiation, and migration of T cells and neutrophils and is crucial for macrophage activation and phagocytosis [35,65,66]. Remarkably, SELENOK is highly expressed not only in lymphatic tissues and immune cells but also ranks among the top five selenoproteins present in the brain [24,67]. However, the exact role of SELENOK in modulating brain immunity remains unclear. This study elucidated that SELENOK deficiency in the brain compromises microglial immune functions, such as migration and phagocytosis, while significantly lowering inflammatory cytokine levels. These findings indicate the pivotal role that SELENOK plays in orchestrating brain immune responses via microglia. Intriguingly, overexpressing SELENOK in normal microglia does not influence their cytokine profile, highlighting its potential in preserving brain immune homeostasis and affirming its importance in immune maintenance

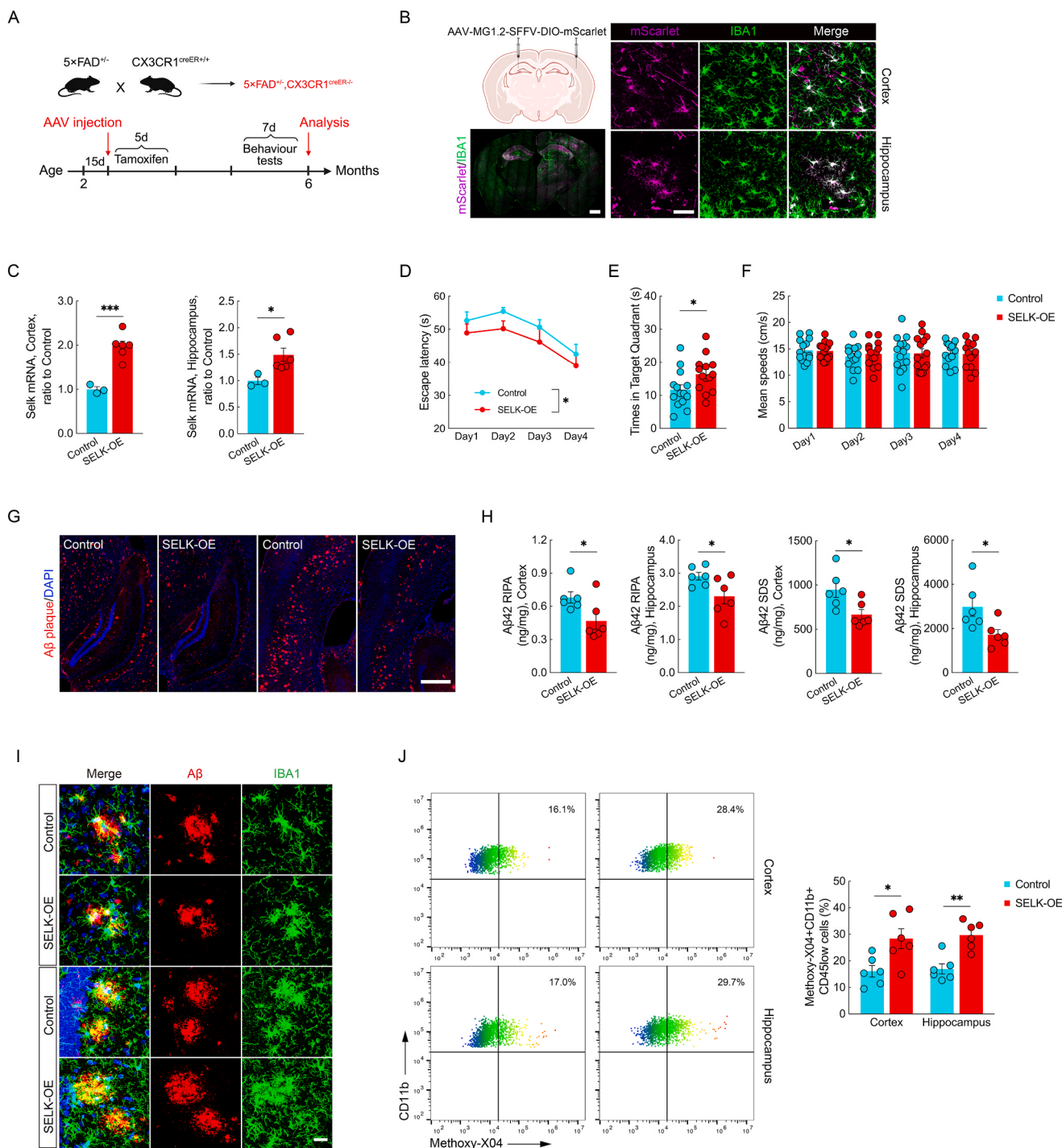


**Fig. 5.** Enhanced A $\beta$  phagocytosis and cognitive improvement in AD mice with microglial SELENOK overexpression.

**Fig. 3.** Enhanced A $\beta$  phagocytosis and cognitive improvement in SELK-OE mice with microglial SELENOK overexpression. (A) Schematic diagram for generating heterozygous Cx3cr1 $^{CreER}$ -5xFAD mice and experimental timetable. (B) Representative fluorescence micrographs of positive microglia (purple) injected with AAV-MG1.2 in Cx3cr1 $^{CreER}$ -5xFAD mice. Total microglia were stained with Iba1 (green) as a control. The whole brain, bar = 1000  $\mu$ m. The partial region, bar = 50  $\mu$ m. (C) SELENOK mRNA levels in Cx3cr1 $^{CreER}$ -5xFAD (control; n = 3) and SELENOK-overexpression Cx3cr1 $^{CreER}$ -5xFAD (SELK-OE; n = 6) mice. (D–F) Morris water maze tests were performed with six-month-old control and SELK-OE mice (n = 14 per group; 7 male and 7 female mice). (D) Escape latency time to reach the hidden platform was recorded during the 4-day training. (E) A probe trial was performed 24 h after the last trial of a hidden platform task, and the search time for the target quadrant recorded. (F) Swimming speeds of the two groups were recorded during the tests. (G) Representative immunofluorescence images of the coronal sections of control and SELK-OE mice stained with MOAB-2 (A $\beta$ , red) and DAPI (blue). Bar = 500  $\mu$ m. (H) Quantification of RIPA- and SDS-soluble human A $\beta$ 42 in the cortical and hippocampal samples of five-month-old control and SELK-OE mice using ELISA (n = 6 per group; 3 male and 3 female mice). (I) Representative immunofluorescence of A $\beta$  plaque and microglia from control and SELK-OE mice stained with Iba1 (green), MOAB-2 (A $\beta$ , red), and DAPI (blue). Bar = 20  $\mu$ m. (J) Representative FACS dot plots showing the microglial phagocytosis of A $\beta$  in the cortex and hippocampus of control and SELK-OE mice (left). Percent (%) methoxy-XO4 $^+$ CD11b $^+$ CD45 $^{low}$  microglia isolated from the brain of these two groups of mice were determined using flow cytometry (right) (n = 6 per group; 3 male and 3 female mice). All data are presented as the mean  $\pm$  SEM. Data from (B) were analyzed using two-way ANOVA and Bonferroni post hoc analysis. Other data were analyzed using Student's t-test. \*p < 0.05; \*\*p < 0.01; \*\*\*p < 0.001. (For interpretation of the references to colour in this figure legend, the reader is referred to the Web version of this article.)

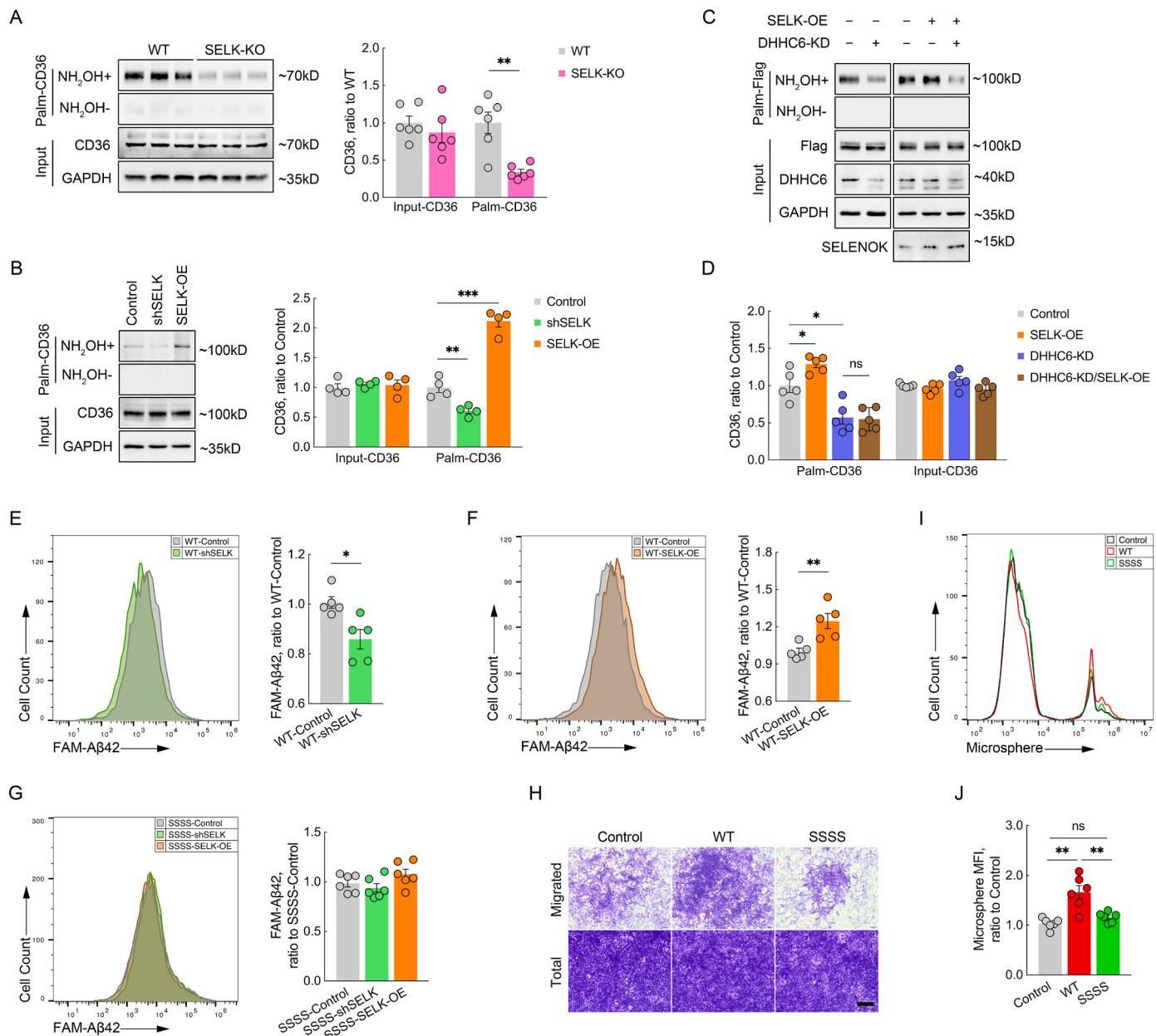


**Fig. 6.** CD36 palmitoylation mediated by SELENOK modulates microglial function and A $\beta$  phagocytosis.

(A) Representative immunoblots and quantification of CD36 protein expression and palmitoylation levels in cortical lysates from 10-month-old wild-type (WT) and SELENOK knockout (SELK-KO) mice. Palmitoylated proteins were enriched by acyl-ABE ( $n = 6$  per group; 3 male and 3 female mice). (B) Representative immunoblots and quantification of CD36 protein expression and palmitoylation levels in control, SELENOK knockdown (shSELK), and SELENOK overexpressing (SELK-OE) primary microglia ( $n = 4$  independent experiments). (C–D) HMC3 cells were transfected with a CD36-Flag plasmid and co-transfected with vehicle (control), shDHHC6 (shDHHC6), ADV-SELK-OE (SELK-OE), or shDHHC6/ADV-SELK-OE (shDHHC6/SELK-OE) plasmids. Representative immunoblots and quantification of CD36-Flag protein expression and palmitoylation levels in all groups of HMC3 cells ( $n = 5$  independent experiments). (E–G) Flow cytometric analysis of A $\beta$  phagocytosis in HMC3 cells. HMC3 cells were transfected with CD36-Flag (WT) or CD36-mutant-Flag (SSSS) plasmid and co-transfected with ADV: vehicle (control), shSELK, or SELK-OE. Representative histogram and summary bar graphs showing frequencies of the cells containing carboxyfluorescein-A $\beta$ 42 (FAM-A $\beta$ 42). (E–F) WT and (G) SSSS groups. ( $n = 5$ –6 independent experiments). (H) Representative images of the migration ability of HMC3 cells transfected with vehicle (control), CD36-Flag (WT), or CD36-mutant-Flag (SSSS) plasmids. Bar = 200  $\mu$ m. (I–J) Representative histogram (I) and summary bar graphs (J) showing frequencies of the cells in (H) containing FAM-A $\beta$ 42 ( $n = 6$  independent experiments). All data are presented as the mean  $\pm$  SEM. Data from (A, E, and F) were analyzed using Student's t-test. Other data were analyzed using one-way ANOVA and Dunnett's multiple comparisons test. \* $p < 0.05$ ; \*\* $p < 0.01$ ; \*\*\* $p < 0.001$ .

of the central nervous system. Therefore, this study provides insights into the role of Se in brain immunity from the perspective of selenoproteins. Emerging research indicates the pivotal involvement of dysfunctional microglia in mediating neuroinflammation, a key factor in various central nervous system disorders and neurodegenerative diseases [68]. This includes the involvement of microglial phagocytosis of pathological proteins, such as synuclein in Parkinson's disease.

Consequently, our results contribute to and substantiates, to a certain extent, the understanding of the therapeutic potential of Se in addressing neuroinflammatory-related diseases.

Numerous genes associated with AD risk are closely associated with microglia [25,69], suggesting that the function of SELENOK in brain immune regulation may also be crucial in the pathology of AD. The advancement in single-cell genomics has brought DAM, identified in AD

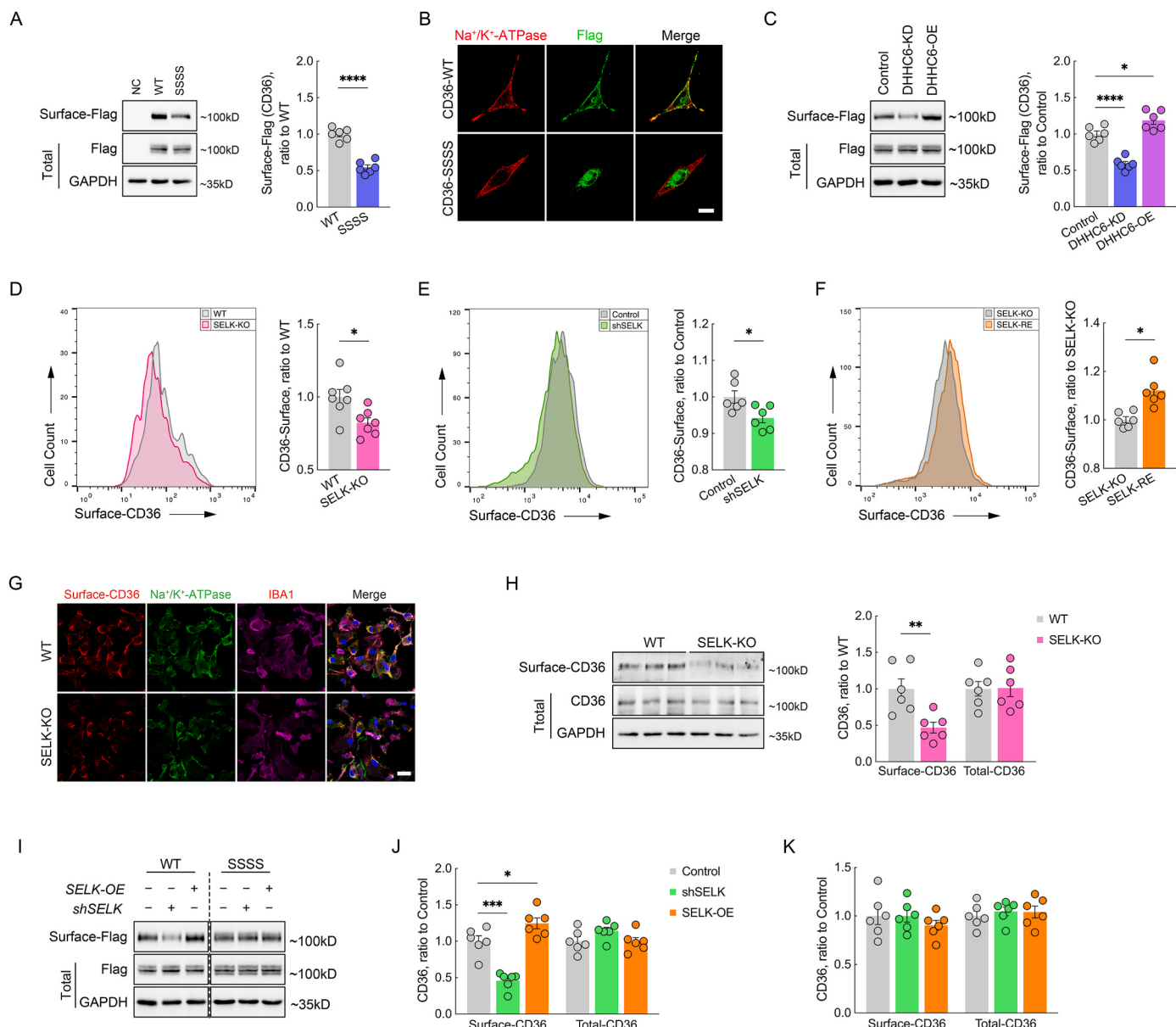
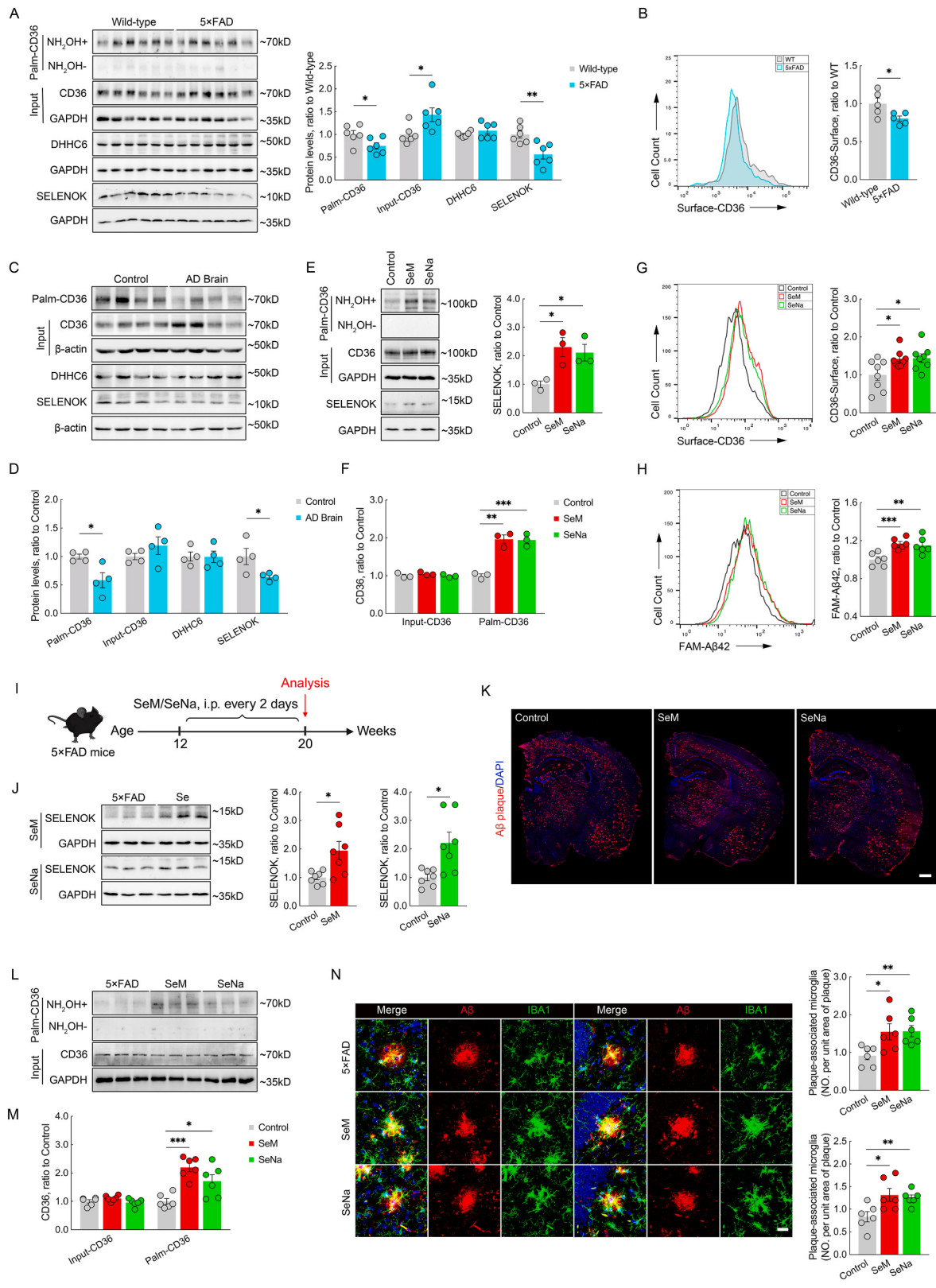


**Fig. 7. SELENOK regulates palmitoylation-driven CD36 localization in microglial plasma membranes.**

(A) HMC3 cells were transfected with vehicle (NC), CD36-Flag (wild-type; WT), or CD36-mutant-Flag (SSSS) plasmids. Representative immunoblots and quantification of Flag expression and surface-Flag levels in lysates from microglial plasma membranes isolated via surface biotinylation ( $n = 6$  independent experiments). (B) Representative immunofluorescence images of cells in (A) stained with Flag (green) and  $\text{Na}^+/\text{K}^+$ -ATPase (red). Bar = 20  $\mu\text{m}$ . (C) HMC3 cells were transfected with a CD36-Flag plasmid and co-transfected with vehicle (control), DHHC6-KD (DHHC6-KD), or DHHC6-OE (DHHC6-OE) plasmids. Representative immunoblots and quantification of Flag expression and surface-Flag levels in lysates from the microglial plasma membrane ( $n = 6$  independent experiments). (D) Flow cytometric analysis of surface-CD36 in FACS-sorted CD45/CD11b $^+$  microglia from brain samples of 10-month-old WT and SELENOK knockout (SELK-KO) mice. Representative histogram and summary bar graphs showing frequencies of the cells stained with CD36 (FITC) ( $n = 7$  per group; 4 male and 3 female mice). (E–F) Representative histogram and summary bar graphs showing frequencies of the cells stained with CD36 (FITC). (E) Primary microglia from WT mice were transfected with ADV-shSELK. Flow cytometric analysis of surface-CD36 in control and SELENOK knockdown (shSELK) primary microglia. (F) Primary microglia from SELK-KO mice were transfected with ADV-SELK (SELK-RE). Flow cytometric analysis of surface-CD36 in SELK-KO and SELENOK re-expression (SELK-RE) primary microglia ( $n = 6$  independent experiments). (G) Representative immunofluorescence images of WT and SELK-KO primary microglia stained with CD36 (red),  $\text{Na}^+/\text{K}^+$ -ATPase (green), Iba1 (purple), and DAPI (blue). Bar = 20  $\mu\text{m}$ . (H) Representative immunoblots and quantification of CD36 protein expression and surface-CD36 levels in lysates from the plasma membrane of WT and SELK-KO primary microglia ( $n = 6$  independent experiments). (I–K) HMC3 cells were transfected with CD36-Flag (WT) or CD36-mutant-Flag (SSSS) plasmids and co-transfected with ADV harboring vehicle (control), shSELK, or SELENOK overexpressing (SELK-OE) plasmids. Representative immunoblots and quantification of Flag expression and surface-Flag levels in lysates from the microglial plasma membrane. (J) WT and (K) SSSS groups ( $n = 6$  independent experiments). All data are presented as the mean  $\pm$  SEM. Data from (C, J, and K) were analyzed via one-way ANOVA and Dunnett's multiple comparisons test. Other data were analyzed using Student's t-test. \* $p < 0.05$ ; \*\* $p < 0.01$ ; \*\*\* $p < 0.001$ ; \*\*\*\* $p < 0.0001$ . (For interpretation of the references to colour in this figure legend, the reader is referred to the Web version of this article.)



(caption on next page)

**Fig. 8.** Se enhances CD36 palmitoylation and microglial A $\beta$  phagocytosis in AD.

(A) Representative immunoblots and quantifications of CD36, DHHC6, and SELENOK protein expression, as well as CD36 palmitoylation levels, in hippocampal lysates from six-month-old wild-type (WT) and 5xFAD mice ( $n = 6$  per group; 3 male and 3 female mice). (B) Flow cytometric analysis of surface-CD36 in FACS-sorted CD45/CD11b $^{+}$  microglia from brain samples of six-month-old WT and 5xFAD mice. Representative histogram and summary bar graphs showing frequencies of the cells stained with CD36 (FITC) ( $n = 6$  per group; 3 male and 3 female mice). (C–D) Representative immunoblots and quantification of CD36, DHHC6, and SELENOK protein expression, as well as CD36 palmitoylation levels, in the temporal lobe lysates of control patients brains and those with AD ( $n = 4$  per group). (E–H) Primary microglia were treated with 10  $\mu$ M selenomethionine (SeM) or sodium selenite (SeNa) for 48 h before the assay. (E–F) Representative immunoblots and quantification of CD36, SELENOK protein expression, and CD36 palmitoylation levels in primary microglia ( $n = 3$  independent experiments). (G) Representative histogram and summary bar graphs showing frequencies of the cells stained with CD36 (FITC) ( $n = 8$  independent experiments). (H) Representative histogram and summary bar graphs showing frequencies of the cells containing carboxyfluorescein-A $\beta$ 42 (FAM-A $\beta$ 42) ( $n = 6$  independent experiments). (I) Schematic diagram of IP administration of SeM or SeNa in five-month-old 5xFAD mice. (J) SELENOK protein levels in cortical lysates of 5xFAD mice treated with SeM or SeNa ( $n = 6$  per group; 3 male and 3 female mice). (K) Representative immunofluorescence images of coronal brain sections from control, SeM-treated, and SeNa-treated mice stained with MOAB-2 (A $\beta$ , red) and DAPI (blue). Bar = 1000  $\mu$ m. (L–M) Representative immunoblots and quantification of CD36 protein expression and palmitoylation levels in cortical lysates of the brains of control, SeM-treated, and SeNa-treated mice ( $n = 6$  per group; 3 male and 3 female mice). (N) Representative immunofluorescence images of A $\beta$  plaque and microglia of control, SeM-treated, and SeNa-treated AD mice stained with Iba1 (green), MOAB-2 (A $\beta$ , red), CD68 (purple), and DAPI (blue). Bar = 20  $\mu$ m. Number of A $\beta$  plaque-associated microglia are shown on the left ( $n = 3$  per group; six sections; 30 A $\beta$  plaques). All data are presented as the mean  $\pm$  SEM. Data from (A, B, and J) were analyzed using Student's t-test. Other data were analyzed using one-way ANOVA and Dunnett's multiple comparisons test. \* $p < 0.05$ ; \*\* $p < 0.01$ ; \*\*\* $p < 0.001$ ; \*\*\*\* $p < 0.0001$ . (For interpretation of the references to colour in this figure legend, the reader is referred to the Web version of this article.)

brains, into the spotlight of AD and microglia research [45,70]. DAM, known for its active phagocytosis of A $\beta$  plaques, plays a key role in mitigating AD pathology. Therefore, understanding the mechanisms that drive the transformation of homeostatic microglia into DAM has become a crucial aspect of AD research and therapy [34,71]. Transcriptome analysis of adult mouse microglia revealed that SELK-KO microglia and DAM exhibit distinctly divergent transcriptional profiles compared to that of homeostatic microglia, implying that microglial SELENOK deficiency hampers the transition to a DAM phenotype. This hypothesis is further substantiated by a series of A $\beta$  phagocytosis experiments. In vivo investigations confirmed that changes in microglial SELENOK expression directly affect their A $\beta$  phagocytosis and cognitive impairment in AD mice, emphasizing the regulation of SELENOK in AD progression. Importantly, while we had used SELK-KO 5xFAD mice (not microglial SELK-KO mice), comprehensive analyses across various A $\beta$  production and degradation pathways demonstrated that SELENOK affects AD pathology predominantly through the regulation of microglial A $\beta$  phagocytosis.

In mechanistic exploration, the initial analyses of transcriptomic data fell short of yielding anticipated insights. As a result, we steered towards a thorough review and analysis of the biological implications of SELENOK. A critical aspect that we examined was the effects of SELENOK on intracellular Ca $^{2+}$  flux. SELENOK deficiency, mediated via IP3R-associated ER Ca $^{2+}$  stores, leads to an overload of intracellular Ca $^{2+}$ , a state typically associated with cellular stress responses [57, 72–74]. This poses an apparent contradiction to the diminished microglial immune response observed in SELENOK-deficient conditions, suggesting the existence of other pivotal mechanisms that influence microglial function. Moreover, the most extensively reported SELENOK-related mechanism, centered on ER stress [22,75], appears to have a less direct association with its effects on microglia. We, therefore, redirected our focus to studying the impact of SELENOK on microglial functions and A $\beta$  phagocytosis. Our findings suggest that SELENOK depletion diminishes microglial immune responses, potentially due to impaired innate immunity mediated by pattern recognition receptors, which are crucial for the recognition and binding necessary for A $\beta$  phagocytosis by microglia [76]. Among these receptors, we unexpectedly discovered a close relationship between CD36 and SELENOK. SELENOK-dependent CD36 palmitoylation in macrophages significantly influences CD36 stability. This interplay places CD36 at a juncture directly connected with the functionality of SELENOK and microglial A $\beta$  phagocytosis, positioning it as a strategic target for mechanistic exploration.

In this study, we systematically unveiled a comprehensive mechanism whereby SELENOK regulates CD36 palmitoylation through DHHC6, mediating its expression on the microglial plasma membrane and consequently affecting the microglial phagocytosis of A $\beta$ . Notably,

we discerned the specificity of the impact SELENOK has on CD36 in microglia. SELENOK/DHHC6 palmitoylates CD36 to regulate its membrane localization without altering total CD36 expression in microglia. This is also a key aspect of how palmitoylation modification affects protein function [55,59]. As an ER-resident selenoprotein, Hoffmann et al. have extensively reported the interaction of SELENOK with DHHC6 and their joint effect on the palmitoylation of target proteins [56]. However, detailed effects of SELENOK/DHHC6-palmitoylated CD36 on its subsequent localization on the microglial plasma membrane were not addressed in this study. Existing data indicates that proteins are sequentially palmitoylated in the ER and Golgi apparatus before reaching the plasma membrane [77]. In addition to DHHC6, other DHHC enzymes, such as DHHC4 in the Golgi and DHHC5 on the plasma membrane, also contribute to CD36 palmitoylation [61,78]. Therefore, CD36 trafficking from the ER to the plasma membrane is orchestrated by a cascade of DHHC enzymes, with DHHC6 potentially directly influencing its transport to the Golgi. Recent studies exploring the effect of SELENOK on CD36 transport in hepatocytes have affirmed this process [54].

A significant elevation in CD36 expression has been reported in brains with A $\beta$  deposition [79], along with the identification of a high CD36-expressing microglial subtype [34]. Additionally, numerous studies report that increased CD36 expression or recycling significantly enhances the A $\beta$  phagocytosis and degradation of microglia [62,80,81]. These findings underscore the crucial role of CD36 in the functionality of microglia within A $\beta$  pathology. However, to date, there have been no reports on the changes in CD36 palmitoylation within AD microglia or its role in the progression of AD. Our investigations in patients and mouse models with AD have identified a marked reduction in CD36 palmitoylation as a notable pathological change during AD development. Although SELENOK levels are also markedly reduced in AD brains, current evidence does not conclusively establish it as the sole cause of diminished CD36 palmitoylation in AD. Nonetheless, we demonstrated that increasing SELENOK levels in the brain can promote CD36 palmitoylation and strengthen microglial A $\beta$  phagocytosis, as confirmed by our subsequent in vivo and in vitro Se supplementation experiments. Consequently, these findings substantiate a profound mechanism where Se, dependent on SELENOK, regulates microglial functions to ameliorate AD. Given that the human body contains 25 selenoproteins, with seven located in the ER and five highly expressed in the brain [20,67], it is challenging to link the effect of Se to a singular selenoprotein. Multiple selenoproteins may exert similar, synergistic, or antagonistic biological actions within cells. Hence, our study is a significant step forward, despite it not comprehensively elucidating the anti-AD mechanisms of Se. Nevertheless, it confirms that SELENOK is a critical target in the influence of Se on brain immunity and microglia in AD, providing new perspectives for the study of other selenoproteins in

this field and advancing the understanding of Se as a potential therapeutic agent in AD treatment.

### CRediT authorship contribution statement

**Pei Ouyang:** Writing – original draft, Resources, Investigation, Formal analysis, Data curation. **Zhiyu Cai:** Writing – original draft, Resources, Methodology, Investigation, Formal analysis, Data curation. **Jiaying Peng:** Resources, Investigation, Data curation. **Shujing Lin:** Resources, Formal analysis. **Xiaochun Chen:** Investigation. **Changbin Chen:** Investigation. **Ziqi Feng:** Investigation. **Lin Wang:** Methodology. **Guoli Song:** Writing – review & editing, Funding acquisition. **Zhong-hao Zhang:** Writing – review & editing, Writing – original draft, Resources, Project administration, Methodology, Investigation, Funding acquisition, Formal analysis, Data curation, Conceptualization.

### Declaration of competing interest

The authors declare that they have no known competing financial interests or personal relationships that could have appeared to influence the work reported in this paper.

### Data availability

Data will be made available on request.

### Acknowledgments

This work was supported by the National Natural Sciences Foundation of China [grant number 32171223]; the Natural Science Foundation of Guangdong Province [grant number 2021A1515010557]; Shenzhen University 2035 Initiative [grant number 2023C002]; and the Shenzhen Fundamental Research Program [grant number JCYJ20200109105836705]. The authors are extremely thankful to Professor Eryan Kong and Dr. Wei Yuan (Second Affiliated Hospital of Xinxiang Medical University, Henan, China) for their technical assistance in palmitoylated protein detection. We thank Dr. Rui Lin (National Institute of Biological Sciences, Beijing, China) and Professor Minmin Luo (Chinese Institute for Brain Research, Beijing, China) for providing the plasmids used to package the AAV-MG1.2, and also thank the Instrumental Analysis Center of Shenzhen University (Shenzhen, China) for their assistance in our experiments.

### Appendix A. Supplementary data

Supplementary data to this article can be found online at <https://doi.org/10.1016/j.redox.2024.103064>.

### References

- [1] 2023 Alzheimer's disease facts and figures, *Alzheimers Dement* 19 (4) (2023) 1598–1695.
- [2] Y. Zhang, H. Chen, R. Li, K. Sterling, W. Song, Amyloid beta-based therapy for Alzheimer's disease: challenges, successes and future, *Signal Transduct. Targeted Ther.* 8 (1) (2023) 248.
- [3] G.T. Tabor, D.M. Holtzman, Current status of amyloid-targeting immunotherapies for Alzheimer's disease, *Sci. Transl. Med.* 15 (721) (2023) eadk9993.
- [4] M.S. Rafii, P.S. Aisen, Detection and treatment of Alzheimer's disease in its preclinical stage, *Nat Aging* 3 (5) (2023) 520–531.
- [5] W.K. Self, D.M. Holtzman, Emerging diagnostics and therapeutics for Alzheimer disease, *Nat. Med.* 29 (9) (2023) 2187–2199.
- [6] B.R. Cardoso, T.P. Ong, W. Jacob-Filho, O. Jalali, M.I. Freitas, S.M. Cozzolino, Nutritional status of selenium in Alzheimer's disease patients, *Br. J. Nutr.* 103 (6) (2010) 803–806.
- [7] J. Zhou, W. Zhang, Z. Cao, S. Lian, J. Li, J. Nie, Y. Huang, K. Zhao, J. He, C. Liu, Association of selenium levels with neurodegenerative disease: a systemic review and meta-analysis, *Nutrients* 15 (17) (2023).
- [8] R.C. B., D.J. Hare, M. Lind, C.A. McLean, I. Volitakis, S.M. Laws, C.L. Masters, A. I. Bush, B.R. Roberts, The APOE epsilon4 allele is associated with lower selenium levels in the brain: implications for Alzheimer's disease, *ACS Chem. Neurosci.* 8 (7) (2017) 1459–1464.
- [9] S. Gao, Y. Jin, K.S. Hall, C. Liang, F.W. Unverzagt, F. Ma, Y. Cheng, J. Shen, J. Cao, J. Matesan, P. Li, J. Bian, H.C. Hendrie, J.R. Murrell, Selenium level is associated with apoE epsilon4 in rural elderly Chinese, *Publ. Health Nutr.* 12 (12) (2009) 2371–2376.
- [10] X. Du, Q. Shi, Y. Zhao, Y. Xie, X. Li, Q. Liu, J. Iqbal, H. Zhang, X. Liu, L. Shen, S-methylselenocysteine (smc) improves cognitive deficits by attenuating synaptic and metabolic abnormalities in Alzheimer's mice model: a proteomic study, *ACS Chem. Neurosci.* 12 (7) (2021) 1112–1132.
- [11] G. Song, Z. Zhang, L. Wen, C. Chen, Q. Shi, Y. Zhang, J. Ni, Q. Liu, Selenomethionine ameliorates cognitive decline, reduces tau hyperphosphorylation, and reverses synaptic deficit in the triple transgenic mouse model of Alzheimer's disease, *J Alzheimers Dis* 41 (1) (2014) 85–99.
- [12] J. van Eersel, Y.D. Ke, X. Liu, F. Delerue, J.J. Kril, J. Gotz, L.M. Ittner, Sodium selenate mitigates tau pathology, neurodegeneration, and functional deficits in Alzheimer's disease models, *Proc. Natl. Acad. Sci. U. S. A.* 107 (31) (2010) 13888–13893.
- [13] Y. Xie, Y. Tan, Y. Zheng, X. Du, Q. Liu, Ebselen ameliorates beta-amyloid pathology, tau pathology, and cognitive impairment in triple-transgenic Alzheimer's disease mice, *J. Biol. Inorg. Chem.* 22 (6) (2017) 851–865.
- [14] X. Guo, Q. Lie, Y. Liu, Z. Jia, Y. Gong, X. Yuan, J. Liu, Multifunctional selenium quantum dots for the treatment of Alzheimer's disease by reducing abeta-neurotoxicity and oxidative stress and alleviate neuroinflammation, *ACS Appl. Mater. Interfaces* 13 (26) (2021) 30261–30273.
- [15] Z.H. Zhang, Q.Y. Wu, C. Chen, R. Zheng, Y. Chen, Q. Liu, J.Z. Ni, G.L. Song, Selenomethionine attenuates the amyloid-beta level by both inhibiting amyloid-beta production and modulating autophagy in neuron-2a/AbetaPPsw cells, *J Alzheimers Dis* 59 (2) (2017) 591–602.
- [16] Z.H. Zhang, Q.Y. Wu, R. Zheng, C. Chen, Y. Chen, Q. Liu, P.R. Hoffmann, J.Z. Ni, G. L. Song, Selenomethionine mitigates cognitive decline by targeting both tau hyperphosphorylation and autophagic clearance in an Alzheimer's disease mouse model, *J. Neurosci.* 37 (9) (2017) 2449–2462.
- [17] Z.H. Zhang, Q.Y. Wu, C. Chen, R. Zheng, Y. Chen, J.Z. Ni, G.L. Song, Comparison of the effects of selenomethionine and selenium-enriched yeast in the triple-transgenic mouse model of Alzheimer's disease, *Food Funct.* 9 (7) (2018) 3965–3973.
- [18] C. Chen, Y. Chen, Z.H. Zhang, S.Z. Jia, Y.B. Chen, S.L. Huang, X.W. Xu, G.L. Song, Selenomethionine improves mitochondrial function by upregulating mitochondrial selenoprotein in a model of Alzheimer's disease, *Front. Aging Neurosci.* 13 (2021) 750921.
- [19] I. Ingold, C. Berndt, S. Schmitt, S. Doll, G. Poschmann, K. Buday, A. Roveri, X. Peng, F. Porto Freitas, T. Seibt, L. Mehr, M. Aichler, A. Walch, D. Lamp, M. Jastroch, S. Miyamoto, W. Wurst, F. Ursini, E.S.J. Arner, N. Frajedas-Villar, U. Schweizer, H. Zischka, J.P. Friedmann Angeli, M. Conrad, Selenium utilization by GPX4 is required to prevent hydroperoxide-induced ferroptosis, *Cell* 172 (3) (2018) 409–422, e21.
- [20] C. Jehan, D. Cartier, C. Bucharles, Y. Anouar, I. Lihrmann, Emerging roles of ER-resident selenoproteins in brain physiology and physiopathology, *Redox Biol.* 55 (2022) 102412.
- [21] I. Alim, J.T. Caulfield, Y. Chen, V. Swarup, D.H. Geschwind, E. Ivanova, J. Seravalli, Y. Ai, L.H. Sansing, E.J. Ste Marie, R.J. Hondal, S. Mukherjee, J. W. Cave, B.T. Sagdullaev, S.S. Karuppagounder, R.R. Ratan, Selenium drives a transcriptional adaptive program to block ferroptosis and treat stroke, *Cell* 177 (5) (2019) 1262–1279, e25.
- [22] S.Z. Jia, X.W. Xu, Z.H. Zhang, C. Chen, Y.B. Chen, S.L. Huang, Q. Liu, P. R. Hoffmann, G.L. Song, Selenoprotein K deficiency-induced apoptosis: a role for calpain and the ERS pathway, *Redox Biol.* 47 (2021) 102154.
- [23] Z.H. Zhang, C. Chen, S.Z. Jia, X.C. Cao, M. Liu, J. Tian, P.R. Hoffmann, H.X. Xu, J. Z. Ni, G.L. Song, Selenium restores synaptic deficits by modulating NMDA receptors and selenoprotein K in an Alzheimer's disease model, *Antioxidants Redox Signal.* 35 (11) (2021) 863–884.
- [24] Z.H. Zhang, G.L. Song, Roles of selenoproteins in brain function and the potential mechanism of selenium in Alzheimer's disease, *Front. Neurosci.* 15 (2021) 646518.
- [25] R. Guerreiro, J. Bras, J. Hardy, SnapShot: genetics of Alzheimer's disease, *Cell* 155 (4) (2013) 968, 968 e1.
- [26] C.M. Karch, A.M. Goate, Alzheimer's disease risk genes and mechanisms of disease pathogenesis, *Biol. Psychiatr.* 77 (1) (2015) 43–51.
- [27] Z. Fan, D.J. Brooks, A. Okello, P. Edison, An early and late peak in microglial activation in Alzheimer's disease trajectory, *Brain* 140 (3) (2017) 792–803.
- [28] L. Hamelin, J. Lagarde, G. Dorothee, C. Leroy, M. Labit, R.A. Comley, L.C. de Souza, H. Corne, L. Dauphinot, M. Bertoux, B. Dubois, P. Gervais, O. Colliot, M. C. Potier, M. Bottlaender, M. Sarazin, I.t. Clinical, Early and protective microglial activation in Alzheimer's disease: a prospective study using 18F-DPA-714 PET imaging, *Brain* 139 (Pt 4) (2016) 1252–1264.
- [29] Y. Wang, T.K. Ulland, J.D. Ulrich, W. Song, J.A. Tzaferis, J.T. Hole, P. Yuan, T. E. Mahan, Y. Shi, S. Gilfillan, M. Cella, J. Grutzendler, R.B. DeMattos, J.R. Cirrito, D.M. Holtzman, M. Colonna, TREM2-mediated early microglial response limits diffusion and toxicity of amyloid plaques, *J. Exp. Med.* 213 (5) (2016) 667–675.
- [30] F.L. Heppner, R.M. Ransohoff, B. Becher, Immune attack: the role of inflammation in Alzheimer disease, *Nat. Rev. Neurosci.* 16 (6) (2015) 358–372.
- [31] A. Litvinchuk, Y.W. Wan, D.B. Swartzlander, F. Chen, A. Cole, N.E. Propson, Q. Wang, B. Zhang, Z. Liu, H. Zheng, Complement C3aR inactivation attenuates tau pathology and reverses an immune network deregulated in tauopathy models and Alzheimer's disease, *Neuron* 100 (6) (2018) 1337–1353, e5.
- [32] L. Zhong, Y. Xu, R. Zhuo, T. Wang, K. Wang, R. Huang, D. Wang, Y. Gao, Y. Zhu, X. Sheng, K. Chen, N. Wang, L. Zhu, D. Can, Y. Marten, M. Shinohara, C.C. Liu, D. Du, H. Sun, L. Wen, H. Xu, G. Bu, X.F. Chen, Soluble TREM2 ameliorates

- pathological phenotypes by modulating microglial functions in an Alzheimer's disease model, *Nat. Commun.* 10 (1) (2019) 1365.
- [33] C. Gao, J. Jiang, Y. Tan, S. Chen, Microglia in neurodegenerative diseases: mechanism and potential therapeutic targets, *Signal Transduct. Targeted Ther.* 8 (1) (2023) 359.
- [34] H. Ennerfelt, E.L. Frost, D.A. Shapiro, C. Holliday, K.E. Zengeler, G. Voithofer, A.C. Bolte, C.R. Lammert, J.A. Kulas, T.K. Ulland, J.R. Lukens, SYK coordinates neuroprotective microglial responses in neurodegenerative disease, *Cell* 185 (22) (2022) 4135–4152, e22.
- [35] S. Verma, F.W. Hoffmann, M. Kumar, Z. Huang, K. Roe, E. Nguyen-Wu, A.S. Hashimoto, P.R. Hoffmann, Selenoprotein K knockout mice exhibit deficient calcium flux in immune cells and impaired immune responses, *J. Immunol.* 186 (4) (2011) 2127–2137.
- [36] H. Xia, Y. Wang, J. Dai, X. Zhang, J. Zhou, Z. Zeng, Y. Jia, Selenoprotein K is essential for the migration and phagocytosis of immature dendritic cells, *Antioxidants* 11 (7) (2022).
- [37] L. Lv, L. Chai, J. Wang, M. Wang, D. Qin, H. Song, Y. Fu, C. Zhao, J. Jia, W. Zhao, M. Jia, Selenoprotein K enhances STING oligomerization to facilitate antiviral response, *PLoS Pathog.* 19 (4) (2023) e1011314.
- [38] X.L. Meng, C.L. Chen, Y.Y. Liu, S.J. Su, J.M. Gou, F.N. Huan, D. Wang, H.S. Liu, S.B. Ben, J. Lu, Selenoprotein SELENOK enhances the migration and phagocytosis of microglial cells by increasing the cytosolic free Ca(2+) level resulted from the up-regulation of IP3R, *Neuroscience* 406 (2019) 38–49.
- [39] J. Wan, A.F. Roth, A.O. Bailey, N.G. Davis, Palmitoylated proteins: purification and identification, *Nat. Protoc.* 2 (7) (2007) 1573–1584.
- [40] G.N. Huang, W. Zeng, J.Y. Kim, J.P. Yuan, L. Han, S. Muallem, P.F. Worley, STIM1 carboxyl-terminus activates native SOC, I(crac) and TRPC1 channels, *Nat. Cell Biol.* 8 (9) (2006) 1003–1010.
- [41] K. Torii, S. Takagi, R. Yoshimura, S. Miyata, Microglial proliferation attenuates sickness responses in adult mice during endotoxin-induced inflammation, *J. Neuroimmunol.* 365 (2022) 577832.
- [42] D. Nayak, T.L. Roth, D.B. McGavern, Microglia development and function, *Annu. Rev. Immunol.* 32 (2014) 367–402.
- [43] X.L. Meng, C.L. Chen, Y.Y. Liu, S.J. Su, J.M. Gou, F.N. Huan, D. Wang, H.S. Liu, S.B. Ben, J. Lu, Selenoprotein SELENOK enhances the migration and phagocytosis of microglial cells by increasing the cytosolic free Ca(2+) level resulted from the up-regulation of IP(3)R, *Neuroscience* 406 (2019) 38–49.
- [44] M.T. Panayotacopoulou, I. Papageorgiou, M. Pagida, A.E. Katsogridaki, M. Chrysanthou-Piterou, N.A. Valous, N. Halama, E. Patsouris, A. E. Konstantinidou, Microglia activation in the midbrain of the human neonate: the effect of perinatal hypoxic-ischemic injury, *J. Neuropathol. Exp. Neurol.* 81 (3) (2022) 208–224.
- [45] H. Keren-Shaul, A. Spinrad, A. Weiner, O. Matcovitch-Natan, R. Dvir-Szternfeld, T.K. Ulland, E. David, K. Baruch, D. Lara-Astaiso, B. Toth, S. Itzkovitz, M. Colonna, M. Schwartz, I. Amit, A unique microglia type associated with restricting development of Alzheimer's disease, *Cell* 169 (7) (2017) 1276–1290, e17.
- [46] A. Silvin, S. Uderhardt, C. Piot, S. Da Mesquita, K. Yang, L. Geirsdottir, K. Mulder, D. Eyal, Z. Liu, C. Bridlance, M.S. Thion, X.M. Zhang, W.T. Kong, M. Deloger, V. Fontes, A. Weiner, R. Ee, R. Dress, J.W. Hang, A. Balachander, S. Chakarov, B. Malleret, G. Dunsmore, O. Cuxes, J. Chen, S. Garel, C.A. Dutertre, I. Amit, J. Kipnis, F. Ginhoux, Dual ontogeny of disease-associated microglia and disease inflammatory macrophages in aging and neurodegeneration, *Immunity* 55 (8) (2022) 1448–1465 e6.
- [47] Y. Hu, G.L. Fryatt, M. Ghorbani, J. Obst, D.A. Menassa, M. Martin-Estebane, T.A.O. Muntslag, A. Olmos-Alonso, M. Guerrero-Carrasco, D. Thomas, M.S. Cragg, D. Gomez-Nicola, Replicative senescence dictates the emergence of disease-associated microglia and contributes to Abeta pathology, *Cell Rep.* 35 (10) (2021) 109228.
- [48] R. Lin, Y. Zhou, T. Yan, R. Wang, H. Li, Z. Wu, X. Zhang, X. Zhou, F. Zhao, L. Zhang, Y. Li, M. Luo, Directed evolution of adeno-associated virus for efficient gene delivery to microglia, *Nat. Methods* 19 (8) (2022) 976–985.
- [49] Y. Yu, R.D. Ye, Microglial Abeta receptors in Alzheimer's disease, *Cell. Mol. Neurobiol.* 35 (1) (2015) 71–83.
- [50] I.S. Coraci, J. Husemann, J.W. Berman, C. Hulette, J.H. Dufour, G.K. Campanella, A.D. Luster, S.C. Silverstein, J.B. El-Khoury, CD36, a class B scavenger receptor, is expressed on microglia in Alzheimer's disease brains and can mediate production of reactive oxygen species in response to beta-amyloid fibrils, *Am. J. Pathol.* 160 (1) (2002) 101–112.
- [51] Y. Zhao, X. Wu, X. Li, L.L. Jiang, X. Gui, Y. Liu, Y. Sun, B. Zhu, J.C. Pina-Crespo, M. Zhang, N. Zhang, X. Chen, G. Bu, Z. An, T.Y. Huang, H. Xu, TREM2 is a receptor for beta-amyloid that mediates microglial function, *Neuron* 97 (5) (2018) 1023–1031, e7.
- [52] S.D. Yan, X. Chen, J. Fu, M. Chen, H. Zhu, A. Roher, T. Slattery, L. Zhao, M. Nagashima, J. Morser, A. Migheli, P. Nawroth, D. Stern, A.M. Schmidt, RAGE and amyloid-beta peptide neurotoxicity in Alzheimer's disease, *Nature* 382 (6593) (1996) 685–691.
- [53] S. Walter, M. Letiembre, Y. Liu, H. Heine, B. Penke, W. Hao, B. Bode, N. Manietta, J. Walter, W. Schulz-Schiffer, K. Fassbender, Role of the toll-like receptor 4 in neuroinflammation in Alzheimer's disease, *Cell. Physiol. Biochem.* 20 (6) (2007) 947–956.
- [54] M. You, F. Wu, M. Gao, M. Chen, S. Zeng, Y. Zhang, W. Zhao, D. Li, L. Wei, X.Z. Ruan, Y. Chen, Selenoprotein K contributes to CD36 subcellular trafficking in hepatocytes by accelerating nascent COP1 vesicle formation and aggravates hepatic steatosis, *Redox Biol.* 57 (2022) 102500.
- [55] S. Meiler, Y. Baumer, Z. Huang, F.W. Hoffmann, G.J. Fredericks, A.H. Rose, R.L. Norton, P.R. Hoffmann, W.A. Boisvert, Selenoprotein K is required for palmitoylation of CD36 in macrophages: implications in foam cell formation and atherosclerosis, *J. Leukoc. Biol.* 93 (5) (2013) 771–780.
- [56] G.J. Fredericks, P.R. Hoffmann, Selenoprotein K and protein palmitoylation, *Antioxidants Redox Signal.* 23 (10) (2015) 854–862.
- [57] G.J. Fredericks, F.W. Hoffmann, A.H. Rose, H.J. Osterheld, F.M. Hess, F. Mercier, P.R. Hoffmann, Stable expression and function of the inositol 1,4,5-triphosphate receptor requires palmitoylation by a DHHC6/selenoprotein K complex, *Proc. Natl. Acad. Sci. U. S. A.* 111 (46) (2014) 16478–16483.
- [58] G.J. Fredericks, F.W. Hoffmann, R.J. Hondal, S. Rozovsky, J. Urschitz, P.R. Hoffmann, Selenoprotein K increases efficiency of DHHC6 catalyzed protein palmitoylation by stabilizing the acyl-DHHC6 intermediate, *Antioxidants* 7 (1) (2017).
- [59] J. Jin, X. Zhi, X. Wang, D. Meng, Protein palmitoylation and its pathophysiological relevance, *J. Cell. Physiol.* 236 (5) (2021) 3220–3233.
- [60] L. Zhao, C. Zhang, X. Luo, P. Wang, W. Zhou, S. Zhong, Y. Xie, Y. Jiang, P. Yang, R. Tang, Q. Pan, A.R. Hall, T.V. Luong, J. Fan, Z. Varghese, J.F. Moorhead, M. Pinzani, Y. Chen, X.Z. Ruan, CD36 palmitoylation disrupts free fatty acid metabolism and promotes tissue inflammation in non-alcoholic steatohepatitis, *J. Hepatol.* 69 (3) (2018) 705–717.
- [61] J. Wang, J.W. Hao, X. Wang, H. Guo, H.H. Sun, X.Y. Lai, L.Y. Liu, M. Zhu, H. Wang, Y.F. Li, L.Y. Yu, C. Xie, H.R. Wang, W. Mo, H.M. Zhou, S. Chen, G. Liang, T.J. Zhao, DHHC4 and DHHC5 facilitate fatty acid uptake by palmitoylating and targeting CD36 to the plasma membrane, *Cell Rep.* 26 (1) (2019) 209–221, e5.
- [62] J. Xu, T. Yu, E.C. Pietronigro, J. Yuan, J. Arioli, Y. Pei, X. Luo, L. Ye, G. Constantin, C. Mao, Y. Xiao, Pel1 impairs microglial Abeta phagocytosis through promoting C/EBPbeta degradation, *PLoS Biol.* 18 (10) (2020) e3000837.
- [63] J.C. Avery, P.R. Hoffmann, Selenium, selenoproteins, and immunity, *Nutrients* 10 (9) (2018).
- [64] S.J. Fairweather-Tait, T. Filippini, M. Vinceti, Selenium status and immunity, *Proc. Nutr. Soc.* 82 (1) (2023) 32–38.
- [65] R.L. Norton, G.J. Fredericks, Z. Huang, J.D. Fay, F.W. Hoffmann, P.R. Hoffmann, Selenoprotein K regulation of palmitoylation and calpain cleavage of ASAP2 is required for efficient Fc gamma R-mediated phagocytosis, *J. Leukoc. Biol.* 101 (2) (2017) 439–448.
- [66] M.P. Marciel, P.R. Hoffmann, Molecular mechanisms by which selenoprotein K regulates immunity and cancer, *Biol. Trace Elem. Res.* 192 (1) (2019) 60–68.
- [67] Y. Zhang, Y. Zhou, U. Schweizer, N.E. Savaskan, D. Hua, J. Kipnis, D.L. Hatfield, V.N. Gladyshev, Comparative analysis of selenocysteine machinery and selenoproteome gene expression in mouse brain identifies neurons as key functional sites of selenium in mammals, *J. Biol. Chem.* 283 (4) (2008) 2427–2438.
- [68] Y. Wang, L. Cui, H. Zhao, H. He, L. Chen, X. Song, D. Liu, J. Qiu, Y. Sun, Exploring the connectivity of neurodegenerative diseases: microglia as the center, *J. Inflamm. Res.* 16 (2023) 6107–6121.
- [69] C. Sala Frigerio, L. Wolfs, N. Fattorelli, N. Thrupp, I. Voytyuk, I. Schmidt, R. Mancuso, W.T. Chen, M.E. Woodbury, G. Srivastava, T. Moller, E. Hudry, S. Das, T. Saido, E. Karran, B. Hyman, V.H. Perry, M. Fiers, B. De Strooper, The major risk factors for Alzheimer's disease: age, sex, and genes modulate the microglia response to abeta plaques, *Cell Rep.* 27 (4) (2019) 1293–1306, e6.
- [70] Y. Zhou, W.M. Song, P.S. Andhey, A. Swain, T. Levy, K.R. Miller, P.L. Poliani, M. Cominelli, S. Grover, S. Gilfillan, M. Celli, T.K. Ulland, K. Zaitsev, A. Miyashita, T. Ikeuchi, M. Sainouchi, A. Kakita, D.A. Bennett, J.A. Schneider, M.R. Nichols, S.A. Beausoleil, J.D. Ulrich, D.M. Holtzman, M.N. Artyomov, M. Colonna, Human and mouse single-nucleus transcriptomics reveal TREM2-dependent and TREM2-independent cellular responses in Alzheimer's disease, *Nat. Med.* 26 (1) (2020) 131–142.
- [71] S. Wang, R. Sudan, V. Peng, Y. Zhou, S. Du, C.M. Yuede, T. Lei, J. Hou, Z. Cai, M. Celli, K. Nguyen, P.L. Poliani, W.L. Beatty, Y. Chen, S. Cao, K. Lin, C. Rodrigues, A.H. Ellebedy, S. Gilfillan, G.D. Brown, D.M. Holtzman, S. Brioschi, M. Colonna, TREM2 drives microglia response to amyloid-beta via SYK-dependent and -independent pathways, *Cell* 185 (22) (2022) 4153–4169, e19.
- [72] C. Wang, R. Li, Y. Huang, M. Wang, F. Yang, D. Huang, C. Wu, Y. Li, Y. Tang, R. Zhang, J. Cheng, Selenoprotein K modulates intracellular free Ca(2+) by regulating expression of calcium homeostasis endoplasmic reticulum protein, *Biochem. Biophys. Res. Commun.* 484 (4) (2017) 734–739.
- [73] Y. Dong, A.V. Kalueff, C. Song, N-methyl-d-aspartate receptor-mediated calcium overload and endoplasmic reticulum stress are involved in interleukin-1beta-induced neuronal apoptosis in rat hippocampus, *J. Neuroimmunol.* 307 (2017) 7–13.
- [74] J. Zhu, F. Zhou, Q. Zhou, Y. Xu, Y. Li, D. Huang, L. Chen, A. Liu, F. Zou, X. Meng, NLRP3 activation in microglia contributes to learning and memory impairment induced by chronic lead exposure in mice, *Toxicol. Sci.* 191 (1) (2023) 179–191.
- [75] V.A. Shchedrina, R.A. Everly, Y. Zhang, S.P. Gygi, D.L. Hatfield, V.N. Gladyshev, Selenoprotein K binds multiprotein complexes and is involved in the regulation of endoplasmic reticulum homeostasis, *J. Biol. Chem.* 286 (50) (2011) 42937–42948.
- [76] M.T. Heneka, M.J. Carson, J. El Khoury, G.E. Landreth, F. Broszter, D.L. Feinstein, A.H. Jacobs, T. Wyss-Coray, J. Vitorica, R.M. Ransohoff, K. Herrup, S.A. Frautschy, B. Finsen, G.C. Brown, A. Verkhratsky, K. Yamanaka, J. Koistinaho, E. Latz, A. Halle, G.C. Petzold, T. Town, D. Morgan, M.L. Shinohara, V.H. Perry, C. Holmes, N.G. Bazan, D.J. Brooks, S. Hunot, B. Joseph, N. Deigendesch, O. Garaschuk, E. Boddeke, C.A. Dinarello, J.C. Breitner, G.M. Cole, D.T. Golenbock, M. P. Kummer, Neuroinflammation in Alzheimer's disease, *Lancet Neurol.* 14 (4) (2015) 388–405.
- [77] J. Greaves, L.H. Chamberlain, Palmitoylation-dependent protein sorting, *J. Cell Biol.* 176 (3) (2007) 249–254.
- [78] J.W. Hao, J. Wang, H. Guo, Y.Y. Zhao, H.H. Sun, Y.F. Li, X.Y. Lai, N. Zhao, X. Wang, C. Xie, L. Hong, X. Huang, H.R. Wang, C.B. Li, B. Liang, S. Chen, T.

- J. Zhao, CD36 facilitates fatty acid uptake by dynamic palmitoylation-regulated endocytosis, *Nat. Commun.* 11 (1) (2020) 4765.
- [79] R. Ricciarelli, C. D'Abamo, J.M. Zingg, L. Giliberto, W. Markesberry, A. Azzi, U. M. Marinari, M.A. Pronzato, M. Tabaton, CD36 overexpression in human brain correlates with beta-amyloid deposition but not with Alzheimer's disease, *Free Radic. Biol. Med.* 36 (8) (2004) 1018–1024.
- [80] K.M. Lucin, C.E. O'Brien, G. Bieri, E. Czirr, K.I. Mosher, R.J. Abbey, D.F. Mastroeni, J. Rogers, B. Spencer, E. Masliah, T. Wyss-Coray, Microglial beclin 1 regulates retromer trafficking and phagocytosis and is impaired in Alzheimer's disease, *Neuron* 79 (5) (2013) 873–886.
- [81] J.B. El Khoury, K.J. Moore, T.K. Means, J. Leung, K. Terada, M. Toft, M. W. Freeman, A.D. Luster, CD36 mediates the innate host response to beta-amyloid, *J. Exp. Med.* 197 (12) (2003) 1657–1666.